AD A116737

①

| REPORT DOCUMENTATION PAGE | | READ INSTRUCTIONS BEFORE COMPLETING FORM |
|---|---|---|
| 1. REPORT NUMBER<br>AFIT/NR 82-3T | 2. GOVT ACCESSION NO.<br>AD-A116737 | 3 RECIPIENT'S CATALOG NUMBER |
| 4. TITLE (and Subtitle) Thermal Radiation from Hot Surfaces Measured by Optical and Calorimetric Methods. | | 5. TYPE OF REPORT & PERIOD COVERED<br>THESIS/DISSERTATION/ |
| | | 6. PERFORMING ORG. REPORT NUMBER |
| 7. AUTHOR(s)<br>Gerald Thomas O'Connor | | 8. CONTRACT OR GRANT NUMBER(s) |
| 9. PERFORMING ORGANIZATION NAME AND ADDRESS<br>AFIT STUDENT AT: University of Arizona | | 10. PROGRAM ELEMENT. PROJECT, TASK AREA & WORK UNIT NUMBERS |
| 11. CONTROLLING OFFICE NAME AND ADDRESS<br>AFIT/NR<br>WPAFB OH 45433 | | 12. REPORT DATE<br>1982 |
| | | 13. NUMBER OF PAGES<br>96 |
| 14. MONITORING AGENCY NAME & ADDRESS(if different from Controlling Office) | | 15. SECURITY CLASS. (of this report)<br>UNCLASS |
| | | 15a. DECLASSIFICATION/DOWNGRADING SCHEDULE |

16. DISTRIBUTION STATEMENT (of this Report)

APPROVED FOR PUBLIC RELEASE; DISTRIBUTION UNLIMITED

17. DISTRIBUTION STATEMENT (of the abstract entered in Block 20, if different from Report)

LYNN E. WOLAVER
Dean for Research and
Professional Development

18. SUPPLEMENTARY NOTES

APPROVED FOR PUBLIC RELEASE: IAW AFR 190-1 AIR FORCE INSTITUTE O TECHNOLOGY (ATC)
WRIGHT-PATTERSON AFB, OH 45433

22 JUN 1982

19. KEY WORDS (Continue on reverse side if necessary and identify by block number)

20. ABSTRACT (Continue on reverse side if necessary and identify by block number)

ATTACHED

82 07 07 055

DTIC
ELECTE
JUL 1 2 1982
S
E
D

DD FORM 1473 1 JAN 73    EDITION OF 1 NOV 65 IS OBSOLETE          UNCLASS

52-37

THERMAL RADIATION FROM HOT SURFACES

MEASURED BY OPTICAL AND CALORIMETRIC METHODS

by

Gerald Thomas O'Connor

A Thesis Submitted to the Faculty of the

COMMITTEE ON OPTICAL SCIENCES (GRADUATE)

In Partial Fulfillment of the Requirements
For the Degree of

MASTER OF SCIENCE

In the Graduate College

THE UNIVERSITY OF ARIZONA

1 9 8 2

APPROVAL BY THESIS DIRECTOR

This thesis has been approved on the date shown below:

_____          _____
B. O. SERAPHIN                                    Date
Professor of Optical Sciences

ACKNOWLEDGMENTS

# TABLE OF CONTENTS

# LIST OF ILLUSTRATIONS

LIST OF ILLUSTRATIONS—Continued

LIST OF TABLES

ABSTRACT

The radiative heat loss from a surface is determined by its total hemispherical emittance, which consequently plays an important role in aerospace and solar applications. This study compares emittances measured calorimetrically with values derived from near normal incidence spectral reflectance measurements. This optical derivation is based on a number of assumptions which limit the accuracy if not sufficiency fulfilled. These assumptions include sample specularity, a straybody character beyond the range of measurement, only small variations of emittance with temperature, and a perfectly smooth sample surface. The comparison of calorimetrically and optically derived emittance performed in this study not only quantifies the errors introduced by insufficient fulfillment of the assumptions but also identifies which assumption causes the dominant error. The calorimetric emissometer, constructed for this study and based on a heat flow sensor, was calibrated with aluminum and nickel thin films, resulting in good agreement with literature values. New data were obtained on "Black Molybdenum", a material promising for solar photothermal conversion produced by chemical vapor deposition. The study reports emittance values of a set of Black Molybdenum samples differing in their oxygen content, and thus varying in the values of their spectral selectivity.

CHAPTER 1

INTRODUCTION

The interaction of radiation with matter is described by two
optical constants, the refractive index n, and the extinction coeffi-
cient k. The complementary process, the emission of thermal radiation
from materials, is also determined by these two optical constants.
Consequently, the energy transfer between surfaces by means of radiation
can be expressed in terms of n and k.

The accuracy with which these optical constants can be extracted
from the observables, absorptance, $\alpha$, reflectance, $\rho$, transmittance, $\tau$,
and emittance, $\varepsilon$, depends on the spectral range, the optical properties
of the material under consideration, and the characteristics of the
radiating surface. Many studies have been made of various materials to
determine these optical constants, but the results have been con-
tradictory. For example, the Handbook of Chemistry and Physics in two
different editions quotes values for platinum that "differ by a factor
of 8 in refractive index and 2.8 in the extinction factor" (Siegel and
Howell, 1972). New, significant applications of thermal radiation have
been envisioned but require improved knowledge of these constants. It
is important that improved methods of determining them be developed.

Modern technology is especially concerned with energy transfer
by means of thermal radiation. Radiation is the primary method of heat

1

dissipation of reentering space vehicles and high speed aircraft. The space shuttle also has radiative panels for heat dissipation in space which are deployed when the cargo doors are opened. These panels must not only radiate heat away from the shuttle, but also not absorb solar radiation to the point that they add heat to the system. This requires the panels to have optical properties that maximize thermal emittance.

A more difficult task is faced in solar photothermal conversion. Here a solar collector must absorb solar radiation, and suppress re-radiation as it heats up. In high-temperature conversion systems, the task of suppressing the thermal reradiation is far more difficult than improving absorption. According to Carnot's principle, the higher the converter temperature, the more efficiently the incident solar radiation is converted to thermal energy. Thermodynamics dictates, however, that all materials reradiate increasingly more energy as their temperature rises. Finally an equilibrium temperature is reached, where the convert-er radiates away as much energy as it absorbs. Thus, the desired high temperatures for efficient energy conversion will be reached only if the thermal radiation is suppressed. Solar converters require new materials that will both absorb strongly in the solar spectrum and yet radiate very little in the thermal infrared.

The above two samples emphasize the importance of absorptance and emittance of radiating surfaces. Characterizing performance in either application requires the determination of the optical properties of the components. These properties, like all the observables, are functions of the optical constants, $n$, and $k$. As functions of common variables, these observables are interrelated. Current methods of

measuring these properties make use of these interrelationships,
measuring one quantity to compute another.

This study addresses the problems arising in the determination of
total hemispherical emittance. This property can be obtained by several
means, one of which is a near-normal incidence spectral reflectance
measurement. This measurement is used predominantly by the Solar Energy
Group, Optical Sciences Center, University of Arizona, to provide the
necessary spectral information required in the development of solar
collector materials. However, it is questionable whether or not an
accurate determination of the total hemispherical emittance is obtain-
able with only this data. To convert a near-normal incidence spectral
reflectance measurement into a total hemispherical emittance value,
certain assumptions must be made. These assumptions are:

    (1)   specular surface, smooth with respect to wavelength

    (2)   purity, in that there are no contaminants, oxide layers, etc.

    (3)   knowledge of n and k over the infrared region.

These conditions will rarely be fulfilled. As a result, the evaluation
of total radiative loss, based on total hemispherical emittance derived
from a near-normal incidence spectral reflectance, may only be approxi-
mate.

This study evaluates the total radiative loss as derived by a
near-normal incidence spectral reflectance measurement and compares it
to the value determined experimentally by a calorimetric method. The
calorimetric method directly measures the total hemispherical emittance

and so provides the standard against which the optical derivation can be compared.

The test material for this study is a promising new material for high-temperature solar photothermal conversion developed by the Solar Energy Group at the Optical Sciences Center. It consists of a mixture of molybdenum and molybdenum dioxide which has been named "Black Molybdenum". This material has a high solar absorptance and low thermal emittance in a simple durable thin film deposited by Chemical Vapor Deposition (CVD), a process that may be expanded to large scale manufacturing. In order to evaluate fully the photothermal performance of this material, the total hemispherical emittance must be determined.

The three objectives of this thesis are:

(1) An evaluation of the total radiative heat loss as derived trom a near normal incidence spectral reflectance measurement and as compared with a direct calorimetric measurement. The evaluation includes the theory behind the derivation of total hemispherical emittance from a reflectance measurement and a discussion of why this derivation may sometimes give only approximate results.

(2) A confirmation of the total hemispherical emittance of "Black Molybdenum", a promising solar converter material,

(3) A report on the construction of the Calorimetric Vacuum Emissometer (CVE) used in these measurements.

CHAPTER 2

SPECTRAL SELECTIVITY

A solar converter must have a high absorptance in the spectral region where solar radiation is strong and a low emittance in the thermal infrared to be spectrally selective. The purpose of this spectral selectivity is to elevate the equilibrium temperature of the converter to a point where the Carnot efficiency is high. If the converter cannot easily radiate infrared while absorbing solar radiation, the converter's temperature must rise until it starts radiating shorter wavelengths in sufficient quantity to reach thermal equilibrium. The diagram on the next page (Figure 2.1) illustrates spectral selectivity by a step function located at two microns. At wavelengths longer than two microns, the optimum converter has a zero emittance while at wavelengths shorter than two microns this same converter absorbs completely. A blackbody at the normal operating temperature of a solar converter will emit 95% of its radiation at wavelengths longer than two microns. If the converter's emittance approaches zero in this region, the converter will not radiate easily. Also, 95% of the energy in solar radiation is at wavelengths shorter than 2 microns, so the largest part of the available solar energy will be absorbed. This justifies the location of the step at 2 microns (Seraphin, 1981).

One way to compare solar converters is based on thermal efficiency η; one definition of which is

5
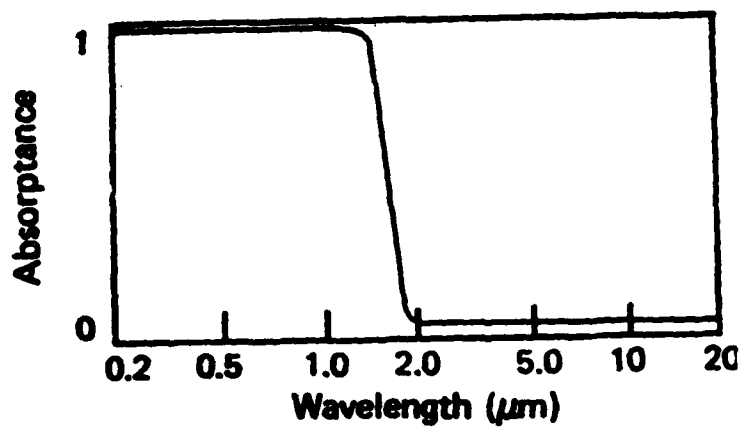
Figure 2.1.  Optimum solar converter spectral porfile with
high absorptance at wavelengths shorter than
2 microns and low emittance at wavelengths
longer than 2 microns.

$$\eta = \frac{Q_{abs} - Q_{rerad} - Q_{conv} - Q_{cond}}{Q_{incident}} \qquad (2.1)$$

where $Q_{abs}$ is the heat absorbed, $Q_{rerad}$ the energy reradiated, and $Q_{conv}$ and $Q_{cond}$ the heat losses due to convection and conduction. $Q_{incident}$ is the total energy incident on the converter. This thesis is concerned with the evaluation of the optical properties of surfaces, in particular the absorptance and emittance. The reduction of convective and conductive losses are primarily engineering problems and so are not pertinent to this thesis; they will be ignored in further discussion. Thus, the purely radiative thermal efficiency is

$$\eta = \alpha_s - \frac{1}{\phi \tau X} [F(\varepsilon_{t_1}, \varepsilon_{t_2})(T_1^4 - T_2^4)] \qquad (2.2)$$

where

$\alpha_s$ = Solar absorptance

$\varepsilon_{t_1}$ = Thermal emittance of absorber surface

$\varepsilon_{t_2}$ = Thermal emittance of environment surrounding absorber surface

$F(\varepsilon_{t_1}, \varepsilon_{t_2})$ = Function of $\varepsilon_{t_1}$ and $\varepsilon_{t_2}$ determined by receiver geometry and orientation

$\sigma$ = Stefan-Boltzmann constant (5.6 x 10 8 W m~-2 k~4

$\tau$ = Transmittance through system optics

$\phi$ = Insolation (direct for most concentrating systems)

$T_1$ = Surface temperature of the absorber surface

$T_2$ = Temperature of environment surrounding receiver

The concerntration factor X is given by

$$X = E \rho \, Ac/Ar \tag{2.3}$$

where

Ac = Effective aperture area of concentrator mirror or lens

Ar = Reradiating area of external reciever

E = (1-e) where e is the fraction of energy lost due to mirror surface imperfections and sun tracking errors

ρ = Specular reflectance of mirror surface within the maximum useful cone angle

As a final similification, $\eta$ reduces to

$$\eta = \alpha_s - \beta \epsilon_t \tag{2.4}$$

where

$$\beta = \frac{\sigma \, [T_1^4 - T_2^4]}{\phi \, \tau \, E \, \rho \, Ac/Ar} \tag{2.5}$$

Thermal efficiency has now been defined in terms of spectral selectivity and in parameters that depend on the characteristics of the system. For different applications, the importance of maximizing $\alpha_s$ as opposed to minimizing the thermal emittance $\epsilon_t$ varies. A small $\beta$ implies that reradiation losses are minimal and $\alpha_s$ should be maximized. A large $\beta$ implies that good spectral selectivity is critical. The figure on the next page (Figure 2.2) shows the benefits of spectral selectivity for systems of different concentration factors, X operating at different temperatures. Spectrally selective converters, which generally sacrifice a small amount of absorptance to obtain the low
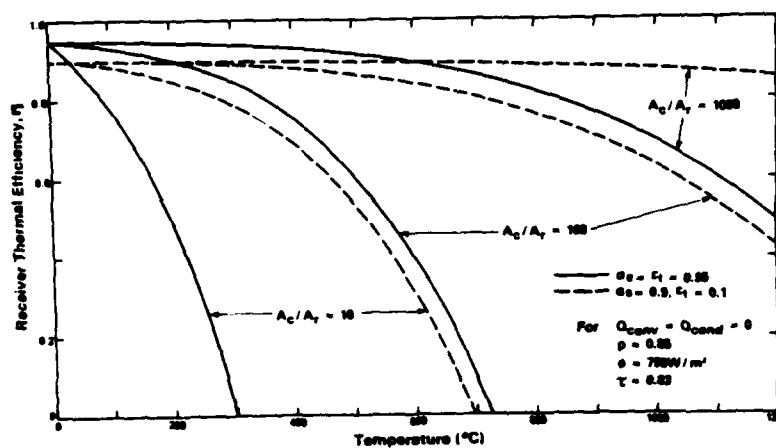
Figure 2.2. Receiver thermal efficiency, η, as a function of temperature, and showing the advantage of spectrally selectivesystems for different concentration factors (Seraphin, 1981).

emittance, drastically outperform non-selective systems at the lower temperatures and intermediate concentration factors (Seraphin, 1981).

There are several physical mechanisms by which spectral selectivity can be generated. Some of these mechanisms are not fully understood. This is the result of the difficulty in separating these mechanisms for individual study and the lack of attempts to do so. The effort must be made, however, so that a systematic design of an optimum converter can be accomplished. Even then, it will probably take the tandem action of several mechanisms to produce sufficient selectivity.

Metals generally have the high infrared reflectance required for low thermal emittance. However, their solar absorptance is inadequate for good selectivity. The emittance and absorptance of metals is a function of the metal's free and bound electrons, respectively. Since the transition metals and rare earths have a large variety in free and bound states, they deserve further investigation. In fact, this is one reason molybdenum was studied by the Optical Sciences Center.

One way to boost the solar absorptance of metals is to overcoat them with a thin film of high absorptance in the visible and near infrared but transparent in the thermal infrared region. This con-figuration is called a dark mirror. Semiconductors are frequently chosen for this task, since interband transitions of electrons provide the necessary absorptance while the material is transparent to the infrared. When the semiconductor absorbs solar photons, it heats the lower metallic layer, which has the necessary low thermal emittance to retain the heat. The semiconductor must be specifically chosen for the

spectral location of the absorption edge. This bilayer converter must also be made antireflective by an interference coating or surface texture to reduce front surface reflection losses.

Another bilayer configuration is the heat mirror. Here, a selective reflector covers the absorber. The absorber can now have a high absorptance over a range larger than just the solar sepctrum, since the reflector is responsible for the selectivity. The reflector must have a high transmittance in the solar spectrum but have a high infrared reflectance. This configuration traps the heat in the absorber, while the selective reflector on top suppresses the thermal reradiation loss. This method is not used as often as the dark mirror or other methods.

Multilayer interference coatings themselves can be used to provide the necessary solar absorptance. Very high selectivity has been achieved in this manner but the "tuned cavity" character of an inter- ference filter makes it sensitive to degradation by slight changes of several parameters. Long-term deterioration from high temperature operation, sensitivity of performance to angle of incidence, and cost and complexity of manufacture discourage the use of interference filters.

Surface texture can greatly assist absorption and interference. There are three basic effects, depending roughly on the wavelength of light. Grooves and pores can increase the effective absorbing area by multiple reflections. These surfaces distinguish between the wave- lengths, absorbing in the solar region but appearing smooth and reflec- tive in the infrared. Manipulating the index of refraction by introducing a sufficient density of voids defines the second category.

Resonant scattering is the third textural effect, where very small particles embedded in a host matrix can, depending on the optical properties of the particles and the matrix, approximate the desired spectral profile by quantum effects.

The Solar Energy Group in the Optical Sciences Center, with which this work was completed, became interested in molybdenum thin films for several reasons. Like most metals, molybdenum has a high infrared reflectance. It has a high melting point, which means it does not agglomerate when used at solar converter operating temperatures. It is refractory, which means it is able to be heated to a very high degree without changing chemically or becoming soft. Molybdenum can be prepared in the thin film form, bypassing the expense of using large quantities of molybdenum. Finally, molybdenum has a lower visible reflectance, i.e., higher solar absorptance, than most metals, thus making it a good candidate for high spectral selectivity.

The CVD process was used to keep the eventual cost of manufacture down. At first the CVD molybdenum thin films did not approach the reflectance of bulk or sputtered molybdenum. It was then discovered that a high temperature anneal (800 C) for thirty minutes resulted in a thin film of relatively pure molybdenum. By varying the CVD process parameters and the annealing time, molybdenum thin films were finally produced that had a reflectance even higher than bulk molybdenum. These films, although containing traces of oxygen and carbon, were dubbed "Super Moly" because of their high reflectance.

The drastic change of the optical properties of molybdenum caused by annealing was an area of intense interest. It was found that during the annealing process, the infrared reflectance improved faster than the solar absorptance diminished. Stated another way, this meant the solar absorptance to infrared emittance ratio could be controlled and maximized. These thin films of partially annealed molybdenum were titled "Black Molybdenum", because of a black or smoky appearance to the eye.

"Black Molybdenum" is a mixture of individual metallic clusters embedded in a host matrix of the dielectric molybdenum dioxide. Figure 2.3 is a photograph taken with a scanning electron microscope of the surface of Black Molybdenum. This composite material can be adjusted over a range of absorptance-emittance values by varying the CVD process parameters and the annealing time and temperature. The advantage of "Black Molybdenum" over "Super Moly" in thin film stacks is simplicity. Although "Super Moly" has a lower infrared emittance, it must be over-coated with a selective absorber to be used in the dark mirror con-figuration. Both forms of molybdenum must then be overcoated with a passivator to prevent long-term degradation. The "Black Molybdenum" only needs one additional layer, as opposed to the two needed by "Super Moly". This simplicity lowers cost and improves durability, as the more layers in a stock, the higher the probability of deterioration. It was also found that the absorptance of "Black Molybdenum" could be further enhanced by chosing the thickness of the passivator layer to act as a single interference layer.

TRANSMISSION ELECTRON MICROGRAPHS OF BLACK MOLYBDENUM

200 nm

200 nm

Figure 2.3. Transmission electron micrographs of Black Molybdenum.

14

The performance of these samples was determined by spectral reflectance measurements. Spectral reflectance measurements provided the necessary spectral information to compare the test material with the step function profile described in this chapter. The spectral reflectance, however, is only indirectly correlated with the total radiative loss of the sample; the total hemispherical emittance is the needed quantity. Although relationships do exist between reflectance and emittance, these relationships are not always valid. The actual thermal emittance of a complex surface, such as these molybdenum thin films, could be quite different than the reflectance measurements suggest. This thesis now provides a direct method for emittance measurement un-hampered by surface structure and other assumptions or approximations. The next chapter wi . discuss the optical observables, emittance, absorptance, and reflectance, and relationships between them for the purpose of showing the potential errors caused by indirect measurement methods.

CHAPTER 3

OPTICAL PROPERTIES AND THEIR INTERRELATIONSHIPS

The three optical quantities of absorptance, emittance, and
reflectance will be discussed in this chapter.  They are observable
characteristics of the optical constants, n and k.  Since they are all
functions of the same variables, it is reasonable to expect relation-
ships among them.  This chapter will define these three observables and
show some relationships among them.  Since most quoted values for
emittance and absorptance are not the result of direct measurement, a
strong understanding of the interrelationships of absorptance, emittance,
and reflectance is necessary to evaluate the validity of the measurement
method.  This evaluation will be described in the next chapter.

## Properties of Blackbodies

Emittance is measured against a fictional standard, called a
blackbody.  A blackbody is a material whose surface is a perfect absorb-
er of all incident radiation at all wavelengths.  Although some materials
can approach blackbody performance in some spectral regions, no real
blackbody exists.  Consider a blackbody in a cavity surrounded by a
material whose surface is also a blackbody and is otherwise perfectly
insulated from the rest of the world.  The enclosed blackbody absorbs
all the radiation from the walls and the walls absorb all the radiation
from the enclosed blackbody.  The Second Law of Thermodynamics requires

16

that the net flow of energy must be from the warmer body to the cooler
one.  Therefore, the blackbody and the surrounding material must come
to thermal equilibrium.  Since, by definition, a blackbody absorbs all
incident radiation, each blackbody in thermal equilibrium must emit as
much as it absorbs  at each wavelength.  Therefore, blackbodies are said
to be perfect emitters, and emittance of non-blackbodies is measured as
the fraction of radiant energy that would be emitted by a blackbody
under similar conditions.

The enclosed blackbody can also show that blackbodies are
perfect emitters in each direction and at every wavelength.  It can also
be shown that the enclosed radiation field is isotropic.  More important-
ly, since the absorbed and emitted radiant energy are equal only when
the blackbody is at thermal equilibrium, without further conditions, it
is therefore apparent that blackbody radiation is only a function of
temperature.

The spectral qualities of a blackbody are described by several
formulae.  The wavelength dependence is given by Planck's spectral
distribution, according to which the spectral exitance of a blackbody
energy per unit area per unit wavelength is

$$M_{e\lambda} = \frac{2\pi hc^2}{\lambda^5}\left[\frac{1}{e^{hc/\lambda KT}-1}\right] \quad . \tag{3.1}$$

The derivation of this equation is associated with the beginnings of
quantum mechanics. The peak of this curve, the primary wavelength
associated with any specific temperature, is given by Wien's Displacement
Law,

$$\lambda T = 2898 \; \mu m \; K \qquad (3.2)$$

If Planck's distribution is integrated over all wavelengths, the
temperature dependence of the total radiant power per area can be cal-
culated. This is the Stefan-Boltzmann Law, which for a blackbody can
be written as

$$M = \sigma T^4 \qquad (3.3a)$$

where M is the total exitance and $\sigma$ is the Stefan-Boltzmann constant.
Real materials, unlike blackbodies, are not perfect radiators at all
frequencies and in all directions. The amount of radiation they emit
is always less. This is where the definition of emittance appears. The
ratio of the radiated power of a real surface to the power radiated from
the same area of a blackbody at the same temperature is called emittance.
The Stefan-Boltzmann equation can be modified for use with real surfaces
by including this factor:

$$M = \epsilon \sigma T^4 \qquad (3.3b)$$

## Emittance and Absorptance

Emissivity is the material's intrinsic ability to radiate. Emittance, on the other hand, is the measured quantity of a sample, which can vary from an emissivity for several reasons, such as surface roughness and oxide layers. Emittance is dependent on body temperature, wavelength, and angle at which the energy is being emitted. $\varepsilon_\lambda{'}(\lambda,\theta,\phi,T)$ is a directional spectral emittance, where the direction is specified by $\theta$ and $\phi$, the elevation and azimuth angles, the wavelength by $\lambda$, and the temperature by T.[1] Emittance can also be averaged over wavelength, direction, or both. Thus one can also speak of directional total emittance $\varepsilon'$ hemispherical spectral emittance, $\varepsilon_\lambda$, or total hemispherical emittance $\varepsilon$. It is this quantity, total hemispherical emittance, that is used in the Stefan-Boltzmann equation for real surfaces.

In the same manner, absorptivity is the ideal property of a real material; absorptance is the measured quantity. Absorptance is slightly more complicated than emittance, however, because in addition to the material, the incident radiation must also be considered, like

---

1. To specify precisely the optical constants of real materials, a convention must be used, because of the large number of independent variables involved. The notation used in this paper is adopted from Siegel and Howell's book, Thermal Radiation Heat Transfer. Functional notation is used to show upon which variables a quantity depends, e.g., $\varepsilon_\lambda{'}(\lambda,\theta,\phi,T)$ shows a dependence on the four variables noted. Since the radiative properties depend on direction, primed quantities represent directional quantities while unprimed quantities represent hemispherical qunatities. The subscripts show a spectral dependence while the absence of a subscript shows that the wavelength dependence has been eliminated. The letter L will be used for radiance and will use the same superscripts, subscripts, and functional form as described above. In addition, radiance may also have the subscripts i, r, and b refering to incident, reflected, or blackbody radiation, respectively. An integration over $2\pi$ implies an intregration over the hemisphere.

emittance, absorptance is a function of wavelength, incident angle, and temperature, and so shares the same modifiers, e.g., directional spectral total hemispherical, etc. Its functional dependence is also shown in the same way, so that $\varepsilon_\lambda{}'(\lambda,\theta,\phi,T)$ is a directional spectral absorptance.

Absorptance and emittance can be even more closely tied together for real materials, if proper care is taken, Kirchhoff's Law is concerned with the relationship between emittance and absorptance for real materials. It is frequently and incorrectly applied by stating absorptance and emittance are equal when the material is at thermal equilibrium with its surroundings. There are times that this is true but only under additional conditions.

## Kirchhoff's Law

Kirchhoff's Law can be applied in several cases. The most general case of Kirchhoff's Law is that at a given temperature, a material's directional spectral emittance and its directional spectral absorptance are equal:

$$\varepsilon_\lambda{}'(\lambda,\theta,\phi,T) = \alpha_\lambda{}'(\lambda,\theta,\phi,T) \tag{3.4}$$

This is a fixed property of all materials and holds without restriction. Kirchhoff's Law also applies to the directional total case. Directional total absorptance can be defined as:

$$\alpha'(\theta,\phi,T) = \frac{\int_0^\infty \alpha_\lambda'(\lambda,\beta,\theta,\phi)\ L'_{\lambda,i}(\lambda,\theta,\phi)\delta\lambda}{\int_0^\infty i'_{\lambda,i}(\lambda,\theta,\phi)\delta\lambda} \qquad (3.5)$$

where $i'_{\lambda,i}(\lambda,\theta,\phi)$ is the incident spectral radiance. By use of Kirchhoff's Law, this can be written as:

$$\alpha'(\theta,\phi,T) = \frac{\int_0^\infty \varepsilon_\lambda'(\lambda,\theta,\phi)\ L'_{\lambda,i}(\lambda,\theta,\phi)\delta\lambda}{\int_0^\infty L'_{\lambda,i}(\lambda,\theta,\phi)\delta\lambda} \qquad (3.6)$$

If the incident radiation has a spectral distribution proportional to that of a blackbody at T, then

$$L'_{\lambda,i}(\lambda,\theta,\phi) = c(\theta,\phi)\ L_{\lambda,b}(\lambda,T) \qquad (3.7)$$

where $c(\theta,\phi)$ is an arbitrary function, and

$$\alpha'(\theta,\phi,T) = \frac{\int_0^\infty \varepsilon_\lambda'(\lambda,\theta,\phi)\ L_{\lambda,b}(\lambda,T)\delta\lambda}{\int_Q^\infty L_{\lambda,b}(\lambda,T)\ \lambda = \sigma T^4/\pi} \qquad (3.8)$$

But, this is the definition of directional total emittance. Therefore, if the incident radiation is proportional to that of a blackbody, then the directional total absorptance equals the directional total emittance.

There is another case where $\alpha'(\theta,\phi,T) = \varepsilon'(\theta,\phi,T)$ is valid. Directional spectral emittance can be defined as

$$\varepsilon_\lambda'(\lambda,\theta,\phi,T) = \frac{L'_\lambda(\lambda,\theta,\phi,T)}{L_{\lambda,b}(\lambda,\theta,\phi,T)} \qquad (3.9)$$

If the directional emitted radiation from the surface is proportional to a blackbody, then,

$$L'_\lambda(\lambda,\theta,\phi,T) = c(\theta,\phi) \, L_{\lambda,b}(\lambda,T) \qquad (3.10)$$

where again $c(\theta,\phi)$ is an arbitrary function. A surface with this kind of behavior is called a directional gray surface. Putting Eq. 3.10 into the definition of directional spectral emittance, Eq. 3.9,

$$\varepsilon_\lambda'(\lambda,\beta,\theta,T) = c(\theta,\phi) \qquad (3.11)$$

The directional spectral emittance is independent of wavelength. This means that the directional total emittance, as defined in the right portion of Eq. 3.8 is also independent of wavelength, i.e., $\varepsilon_\lambda' = \varepsilon'$. From Kirchhoff's Law, $\varepsilon_\lambda' = \alpha_\lambda'$, and from Eq. 3.8 above, $\alpha' = \varepsilon_\lambda'$. Therefore, all four quantities are equal, and especially $\alpha' = \varepsilon'$.

There are also two applications of Kirchhoff's Law for hemispherical spectral absorptance and emittance. Hemispherical spectral absorptance is defined as

$$\alpha_\lambda = \frac{\int_{2\pi} \alpha_\lambda'(\lambda,\theta,\phi,T) \, L_{\lambda,i}(\lambda,\theta,\phi) \, \cos\theta \, \delta\omega}{\int_{2\pi} L'_{\lambda,i}(\lambda,\theta,\phi)\cos\theta \, \delta\omega} \qquad (3.12)$$

where the directional spectral absorptance is integrated over a hemisphere. Using Kirchhoff's Law, this can be rewritten as

$$\alpha_\lambda = \frac{\int_{2\pi} \epsilon_\lambda'(\lambda,\theta,\phi,T)\ L_{\lambda,i}(\lambda,\theta,\phi)\ \cos\theta\ \delta\omega}{\int L_{\lambda,i}'(\lambda,\theta,\phi)\ \cos\theta\ \delta\omega} \tag{3.13}$$

When $\alpha_\lambda'$ and $\epsilon_\lambda'$ are functions of $\lambda, \theta, \phi$, and $T$, $\alpha_\lambda = \epsilon_\lambda$ only if the incident spectral radiance is uniform over all directions, i.e., independent of $\theta$ and $\phi$. This allows the last equation to be rewritten as

$$\alpha_\lambda = \frac{\int_{2\pi} \epsilon_\lambda'(\lambda,\theta,\phi,T)\ \cos\theta\ \delta\omega}{\int_{2\pi} \cos\theta\ \delta\omega} \tag{3.14}$$

The denominator is equal to $\pi$, which turns this equation into the definition of hemispherical spectral emittance:

$$\epsilon_\lambda = \frac{1}{\pi}\ \int_{2\pi} \epsilon_\lambda'(\lambda,\theta,\phi,T)\ \cos\beta\ \delta\omega \quad . \tag{3.15}$$

Therefore, with uniform incident radiance, total hemispherical absorptance equals spectral hemispherical emittance.

The second hemispherical spectral case is derived when the directional spectral quantitites are independent of angle.

$$\begin{aligned}
\epsilon_\lambda'(\lambda,\theta,\phi,T) &= \epsilon_\lambda'(\lambda,T) \\
\alpha_\lambda'(\lambda,\theta,\phi,T) &= \alpha_\lambda'(\lambda,T)
\end{aligned} \tag{3.16}$$

This kind of surface is a diffuse spectral surface, i.e., $\varepsilon_\lambda = \alpha_\lambda$.

Kirchhoff's Law applied to the hemispherical total case is understandably complicated. Hemispherical total quantities are averaged by integrating over both wavelength and angle. Although the order of integration is not important the constraints required to apply Kirchhoff's Law are. Since each integration has two possible requirements to satisfy before applying Kirchhoff's Law, the double integration has four possible combinations under which Kirchhoff's Law applies. The simplest case is the diffuse-gray case, where the directional quantities doe not depend on direction and the spectral quantitites doe not depend on wavelength. Thus,

$$\varepsilon = \varepsilon_\lambda{}' = \alpha_\lambda{}' = \alpha.$$

The above theoretical discussion has omitted one important practical datum. Neither absorptance nor emittance is as easy to measure as is reflectance. However, for opaque bodies, incident radiation is either reflected or absorbed, and with the above relationships between absorptance and emittance, all three quantities can be related. The following discussion will cover the definitions of the various reflectance quantities, and then derive the relationships between the three observables. This will permit us in Chapter 4 to evaluate the use of those relationships to obtain emittance values from reflectance measurements.

## Reflectance

As emittance and absorptance, reflectance is the measured quantity and is a function of the material's reflectivity and surface conditions. The primary reflectance is bidirectional spectral reflectance, $\rho_\lambda{''}(\lambda,\theta_r,\phi_r,\theta,\phi,T)$ where some of the radiation incident at angle $(\theta,\phi)$ will be reflected in the $(\theta_r,\phi_r)$ direction.[2] To find the magnitude of all the reflected radiation, it will be necessary to sum over all possible angles $(\theta_r,\phi_r)$ a hemisphere for a flat surface. Bidirectional spectral reflectance is the ratio of the directional spectral radiance reflected at a specified angle to the spectral radiance incident at another specified angle:

$$\rho_\lambda{''}(\lambda,\theta_r,\phi_r,\theta,\phi,T) = \frac{L_\lambda{''}_{,r}(\lambda,\theta_r,\phi_r,\theta,\phi,T)}{L_{\lambda,i}(\lambda,\theta,\phi)\cos\theta} \quad (3.18)$$

The $\cos\theta$ is required to correct for the amount of energy reflected by the projected area of the surface. For a diffuse reflection, the incident energy from $(\theta,\phi)$ will be distributed evenly around all reflected angles $(\theta_r\phi_r)$. It is also generally true that bidirectional spectral reflectance is symmetric with respect to incident and reflected angles, i.e.,

---

2. Reflectivity is again more complicated than either emissivity or absorptivity, because the direction of the reflected energy must also be specified in addition to the incident direction. The notation already described will be continued, with two additions. A double prime will be used when the reflected direction as well as the incident direction are specified, and the functional notation will also show up to two sets of angles with subscripts to specify reflected variables. Angles not shown have been integrated over the hemisphere.

$$\rho_\lambda{''}(\lambda,\theta_r,\phi_r,\theta,\phi,T) = \rho_\lambda{''}(\lambda,\theta,\phi,\theta_r,\phi_r,T) \qquad (3.19)$$

The next reflected quantities to be discussed specify one angle but sum the over the hemisphere for the other. These quantities are directional hemispherical spectral reflectance, and hemispherical directional spectral reflectance. The directional hemisperical spectral reflectance can be defined as the energy reflected into all solid angles divided by the incident energy from one direction. It is also

$$\rho_\lambda{'}(\lambda,\theta,\phi,T) = \int_{2\pi} \rho_\lambda{''}(\lambda,\theta_r,\phi_r,\theta,\phi,T) \ \cos\theta_r \delta\omega_r \qquad (3.20)$$

The hemispherical directional spectral reflectance is defined as the reflected intensity in the $(\theta_r,\phi_r)$ direction divided by the integrated average incident intensity. There is one important case where these quantities are interchangeable: when the reflectance of a material irradiated at a given angle of incidence $(\theta,\phi)$ as measured by the energy collected over the entire hemisphere of reflection is equal to the reflectance for uniform irradiation from the hemisphere as measured by collecting the energy at a single angle of reflection $(\theta_r,\phi_r)$ and when $(\theta_r,\phi_r)$ is the same angle as $(\theta,\phi)$ (Siegel and Howell, 1972). This important relation is frequently used in integrating sphere reflectometers. Directional spectral absorptance is equal to one minus directional hemispherical spectral reflectance. It is difficult, however, to build a system that will capture all the reflected energy $2\pi$ sterradians. It is possible to build a detector that will detect

the reflected energy in one direction after irradiating the sample with uniform radiation inside a sphere. This is the hemispherical directional spectral reflectance, which can be converted to the directional hemispherical reflectance using the reciprocity relation, and the directional spectral absorptance can then be calculated.

The previous reflectivities have all dealt with spectral radiation. As before, averages taken over wavelength will now be discussed.

Bidirectional total reflectance can be written as

$$\rho''(\theta_r, \phi_r, \theta, \phi, T) = \int_0^\infty \rho_\lambda''(\lambda, \theta_r, \phi_r, \theta, \phi, T) \; L_{\lambda',i}(\lambda, \theta, \phi) d\lambda \quad (3.21)$$

When the spectral distribution of the incident radiation is the same for all directions or even if

$$L_{\lambda,i}(\lambda, \theta, \phi) = c \; L_{\lambda,i}(\lambda) \quad (3.22)$$

with c an arbitrary constant, then

$$\rho''(\theta_r, \phi_r, \theta, \phi, T) = \rho''(\theta, \phi, \theta_r, T) \quad (3.23)$$

Directional total reflectance has the two obvious cases, directional hemispherical and hemispherical directional. Directional hemispherical total reflectance is the fraction of the total energy incident from one direction and reflected into all directions:

$$\rho'(\theta,\phi,T) = \frac{\int_0^\infty \rho_\lambda'(\lambda,\theta,\phi,T)\, L'_{\lambda,i}(\lambda,\theta,\phi)\delta\lambda}{\int_0^\infty L'_{\lambda,i}(\lambda,\theta,\phi)\,\delta\lambda} \qquad . \qquad (3.24)$$

Hemispherical directional total reflectance is the fraction of radiation reflected into one direction from radiation incident from all directions. When the incident radiation is uniform over all directions, the hemispherical directional total reflectance is:

$$\rho'(\theta_r,\phi_r,T) = \frac{\int_0^\infty \rho_\lambda'(\lambda,\theta_r,\phi_r,T)\, L'_{\lambda,i}(\lambda,\theta,\phi)\,\delta\lambda}{\int_0^\infty i'_{\lambda,i}(\lambda)\delta\lambda} \qquad . \qquad (3.25)$$

As in the spectral case, with uniform incident radiation, the two directional total reflectivities are equal:

$$\rho'(\theta,\phi,T) = \rho'(\theta_r,\phi_r,T) \qquad . \qquad (3.26)$$

Finally, the hemispherical total reflectance is fraction of all the incident energy that is reflected. While it is the result of integrations over wavelength and angle, the order of integration is unimportant.

## Interrelationships of Absorptance, Emittance, and Reflectance

Now that all the reflectance quantities have been defined, the relations between them and absorptivity and emissivity can be examined.

For opaque bodies, i.e., no transmission of radiant energy, incident radiant energy is either absorbed or reflected. From this simple relation and Kirchhoff's Law, several further relationships can be written. These are the relationships that make it possible to take a reflectance measurement and obtain an emittance value. These relationships and the conditions under which they apply are important in evaluating the validity of this process.

Consider the case when radiation is incident from a direction $(\theta, \phi)$. For the spectral case, the directional spectral absorptance plus the directional hemispherical spectral reflectance add up to the incident beam:

$$\alpha_\lambda'(\lambda, \theta, \phi, T) + \rho_\lambda'(\lambda, \theta, \phi, T) = 1 \qquad (3.27)$$

Kirchhoff's Law can be applied without restriction to yield:

$$\epsilon_\lambda'(\lambda, \theta, \phi, T) + \rho_\lambda'(\lambda, \theta, \phi, T) = 1 \qquad (3.28)$$

For the total case, the quantitites involved are directional total absorptance and directional hemispherical total reflectance:

$$\alpha'(\theta, \phi, T) + \rho'(\theta, \phi, T) = 1 \qquad (3.29)$$

Kirchhoff's Law for directional total properties can then be applied under the restrictions that the incident radiation is proportional to a blackbody at the same temperature or the surface is directional gray:

$$\epsilon'(\theta,\phi,T) + \rho'(\theta,\phi,T) = 1 \quad . \tag{3.30}$$

There are more relationships between absorptivity, emissivity, and reflectance. They are not, however, pertinent to the discussion in the following material.

This chapter covered the basic definitions of emittance, absorptance, and reflectance, some relationships between them, and the conditions under which those relationships are valid. This will enable us to evaluate current measurements techniques, which will be discussed in the next chapter. We will be able to identify errors caused by the fact that some of the assumptions necessary to make these relationships valid may not always be fulfilled. The next chapter will cover the process of taking a reflectance measurement from a common laboratory instrument and deriving a total hemispherical emittance. Based on the material covered in this chapter, it will be shown that a direct emittance measurement must be made, in order to determine accurately the total radiative loss from a particular surface.

CHAPTER 4 .

EMITTANCE DERIVED FROM REFLECTANCE

Solar photothermal converter performance is often deteimined
more by the total radiative loss than the solar absorptance of the
converter.  An assessment of converter radiative loss requires knowledge
of total hemispherical emittance and the spectral emittance profile
over both the solar and infrared region.  As explained in Chapter 2,
an optimum solar converter material has a spectral profile that is
characterized by a step function with high absorptance at wavelengths
shorter than 2 microns and low emittance at wavelengths longer than
2 microns.  This spectral data is  typically obtained from a spectro-
photometer used in a reflectance mode.  The results of this near normal
incidence spectral reflectance (NNISR) measurement can directly show
the test material's performance as compared to the optimal spectral
profile.  This leaves the total hemispherical emittance of the test
material at operating temperatures of solar converters to be determined.

The total hemispherical emittance of a material can be obtained
by direct measurement.  However, since this quantity is related to
NNISR through the material's optical constants, n and k., it has become
common practice for many groups, including the Solar Energy Group, to
use the NNISR data to obtain the total normal emittance.  The Fresnel
equations can then be modified, if n and k are known, to convert the

31

total normal emittance into total hemispherical emittance.  However,
the assumptions needed to derive total hemispherical emittance from a
NNISR measurement sometimes cause the result to be only approximate.
This chapter will explain the derivation of total hemispherical emittance
from a NNISR measurement, and show, using the relationships developed
in the last chapter, why the accuracy is limited.

The mode of operation of a typical infrared spectrophotometer
must be described to explain how a NNISR measurement is made.  Light
from a broad-band source is formed into a converging cone and reflected
off the sample at an angle near normal, usually 6 to 12 degrees.
Usually, the signal derived from this beam is compared to a signal from
a similar beam reflected off a reference material, e.g., aluminum.  The
results are recorded on a strip chart recorder, as a function of wave-
length.

The first approximation is made in converting this NNISR into a
directional-hemispherical spectral reflectance.  The assumption is made
that all of our samples are specular, i.e., that all reflection is at
angles equal to the angle of incidence.  This assumption allows us to
equate the NNISR to a directional-hemispherical spectral reflectance.
This is equivalent to saying that all the reflected energy in the
hemisphere is assumed to be contained in the small solid angle that
passes through the detector aperture of the infrared spectrophotometer.
No material is perfectly specular; however, some are close.  Specularity
is both a function of the material and of the smoothness of the surface
relative to the wavelength.  Our samples were generally thin films

deposited by CVD, which replicates the well-polished surface of the substrate which is smooth at the infrared wavelengths. This assumption will produce some error, the magnitude of which is proportional to the amount of light scattered out of the specular direction, the light reflected but not collected in the detector aperture.

The directional-hemispherical spectral reflectance is easily converted to directional spectral emittance. Assuming the sample is opaque, Equation 3.28 allows us to write

$$\epsilon_\lambda{}'(\lambda,\theta,\phi,T) = 1 - \rho_\lambda{}'(\lambda,\theta,\phi,T) \qquad (4.1)$$

Since this is a direct application of Kirchhoff's Law, there are no further restrictions. The assumption of opacity is not unimportant, as it was difficult to make uniform samples big enough to be measured in our equipment, and the opacity was especially important in the infrared here the human eye is inadequate to judge. Fortunately, the infrared spectrophotometer used in a transmission mode did prove the samples to be opaque.

It is relatively easy to obtain a directional total emittance from strip chart record planimetry. Planck's blackbody distribution function enables us to calculate the power radiated by a blackbody in each wavelength interval. So, we integrate over wavelength by summing the products of the blackbody power and the directional spectral emittance in small wavelength intervals, and obtain the directional total emittance.

$$\epsilon'(\beta,\theta,T) = \frac{\int_0^\infty \epsilon_\lambda'(\lambda,\beta,\theta,T)Me_\lambda(\lambda,T)\ \delta\lambda}{\sigma T^4} \tag{4.2}$$

If the assumption is made that emittance is a slowly changing function
of temperature, then the integral can be calculated for temperatures
different from those at which the NNISR measurement was made. That is
emittance can be calculated at converter operating temperatures rather
than at room temperatures. Since we know emittance is generally a
slowly varying function of temperature, this assumption introduces only
slight errors. Unfortunately, most infrared spectrophotometers do not
have a large enough spectral range to provide the directional spectral
emittance for all the necessary wavelengths. For example, the Solar
Energy Group uses a Perkin-Elmer 137 spectrophotometer with a range of
2.5 to 15 microns. However, at 150 C, 25% of a blackbody's energy is
contained at wavelengths longer than 15 microns; the necessary long
wavelength limit is approximately 30 microns. In this case, a common
assumption, with associated error, is that the emittance varies little
beyond the last wavelength region measured, so the last value measured
is used over the remaining portion of the integral. This is essentially
a directional gray assumption at long wavelengths. The alternative is to
use blackbody curves for temperatures above 500 C, so that virtually all
the radiated energy is in wavelengths below 15 microns. But then, the
assumption that the room temperature emittance is the 500 C emittance
may break down. These assumptions are not disastrous, but they do make
the result slightly inexact. Nevertheless, we now have a total emit-
tance at near normal angle.

Converting the directional total emittance to a hemispherical total emittance requires the use of the Fresnel equations with their associated limitations and assumptions. These assumptions are simply a smooth surface with no contaminants. The Fresnel equations can be used to derive expressions for both the directional total emittance and hemispherical total emittance in terms of n and k. These take into account the function dependence of emittance on direction; for example, the Brewster angle leak, leading to higher emittance, is incorporated into these expressions. The following equations from Siegel and Howell are for normal total emittance

$$\epsilon_{normal} = \frac{4n}{n^2 + k^2 + 2n + 1} \tag{4.3}$$

and hemispherical total emittance.

$$\epsilon = 4n - 4n^2 \ln \left( \frac{1 + 2n + n^2 + k^2}{n^2 + k^2} \right) + \frac{4n(n^2 - k^2)}{k} \tan^{-1} \left( \frac{k}{n + n^2 + k^2} \right)$$

$$+ \frac{4n}{n^2 + k^2} - \frac{4n^2}{(n^2 + k^2)^2} \ln (1 + 2n + n^2 + k^2) \tag{4.4}$$

$$- \frac{4n(k^2 - n^2)}{k(n^2 + k^2)^2} \tan^{-1} \left( \frac{k}{1 + n} \right)$$

Siegel and Howell also state that for long wavelengths, i.e., greater than microns, n and k can be treated as equal. Having done this, they provide a graph showing the ratio of hemispherical total emittance to normal total emittance as a function of normal total emittance. This graph, Figure 4.1, is shown on the following page.
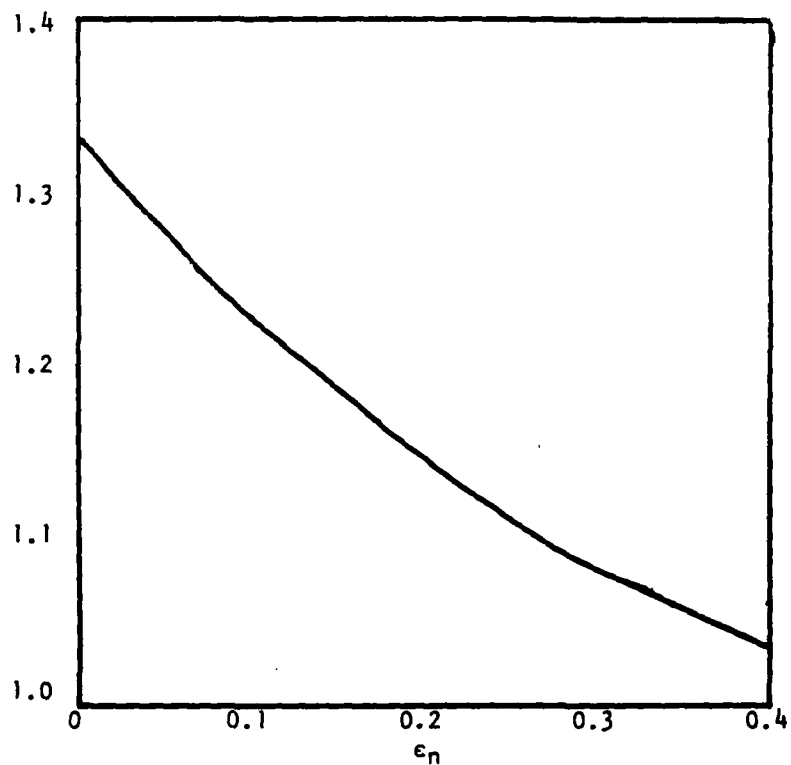
Figure 4.1.  Ratio of total hemispherical emittance to total
normal emittance as a function of total normal
emittance as calculated using the Fresnel equations
in the long wavelength limit where n = k (Siegel
and Howell, 1972).

There are two problems associated with using the Fresnel equations to convert normal emittance to hemispherical emittance. The equations are based on the assumption of a simple, homogeneous substance, which is certainly not the case for complex materials like "Black Molybdenum". Even using average n and k for the composite compounds may not result in the correct ratio. Also, any sample exposed to air soon builds up a thin oxide layer that acts as an anti-reflection coating with angle and wavelength-dependent properties, also affecting the emittance and causing a deviation from the value derived from the Fresnel equations.

This chapter has shown one way of obtaining total hemisperhical emittance from spectral reflectance. This method assumes a smooth specular opaque directional-gray surface free from any contaminants. It also assumes that the sample's emittance is a slowly varying function of temperature. If not fulfilled, these assumptions introduce error into the derived total hemispherical emittance. Because of the uncertainty associated with this method, a direct means of measuring total hemispherical emittance was needed to gauge the accuracy of this indirect optical method. This method is based on the use of the Calorimetric Vacuum Emissometer (CVE), which will be disucssed in the next chapter. The CVE should allow both the direct measurement of emittance, and for any one group of materials, it should allow the computation of a correction factor to the method described in this chapter, so that the emittance from reflectance derived can be inferred with improved confidence.

Chapter 5

CALORIMETRIC EMISSOMETERS

## General Description

The calorimetric measurement of emittance is based on a direct measurement of heat flow into the sample at the equilibrium temperature of the sample.  In this method, the sample is thermally isolated from all heat sources except for a measurable power input.  This is usually accomplished by suspending the sample in an evacuated chamber by thin wires, which limit the heat loss and yet allow electrical resistive heating.  The sample, of course, radiates power according to the Stefan-Boltzmann law; the power radiated by the sample equals the power radiated by a blackbody at the same temperature times the total hemispherical emittance of the sample.  The temperature of the sample can be measured by thermocouples or optical means.  Because of the thermal isolation, the input power must equal the radiated power. Since the input power is known, and the blackbody radiated power as a function of temperature is obtainable, the emittance can be calculated.

$$\varepsilon = \frac{M}{\sigma T^4} \tag{5.1}$$

The requirement for thermal isolation of the sample can be demonstrated by an assessment of the energy balance of the emissometer. The heat flow into the sample is

$$Q(total) = Q(conv) + Q(cond) + Qsc) + Q(a) + Q(h) - Q(r) \qquad (5.2)$$

where Q(conv) is the heat flow due to air convection, Q(cond) is the
heat flow due to heat conduction, Q(sc) is the heat flow from the
supports holding the sample, Q(a) is the heat absorbed from other
radiating surfaces, Q(h) is the heat flow into the sample from a heat
source, and Q(r) is the heat flow out of the sample by radiation. The
Stefan-Boltzmann equation can be used to calculate the emittance if all
the terms in Eq. 5.2 can be made negligibly small compared to Q(h) and
Q(r). Both Q(cond) and Q(conv) become negligible in a high vacuum where
there is insufficient air to transport heat energy. Q(sc) is reduced
by using narrow wires to limit the heat flow, and even then, a correction
factor is usually calculated based on the wires' heat conductivity.
Q(a) requires two actions to minimize it. Even at room temperature,
the walls of the chamber around the sample are radiating appreciable
amounts of energy. The relative effect of this radiation can be reduced
to negligible amounts by either heating the sample well above sample
temperature or by cooling the walls of the chamber to temperatures well
below the sample's temperature. The sample can also absorb reflected
energy, radiated by itself and reflected off the chamber walls. The
walls, therefore, are usually treated to absorb strongly. This leaves
the desired result of a Q(h) that can be accurately measured and a Q(r)
so much larger than the other remaining terms that they can be ignored.
Further discussion of calorimetric emissometers of this description can
be found in a variety of sources (Touloukian and DeWitt, 1970).

The system described in the preceeding section had one drawback for our purposes. The proposed samples were thin films deposited on one side of a substrate, and so the radiative section had to be confined to that one side. This required modifying the usual emissometer. Instead of suspending the sample with wires, the sample was mounted on a block of copper with only the coated side exposed. In between the samples and the block was a thermopile, a collection of themocouples in series on either side of a material of known thermal characteristics, in this case, Kapton™. The thermopile measures heat flow by measuring minute temperature differences between the Kapton surfaces. This not only allowed the direct measurement of the heat flow but eliminated Q(sc) since all heat entering the sample had to enter through the heat flow sensor.

## A Detailed Description of the
## Calorimetric Vacuum Emissometer

The following discussion will cover the actual components of the Calorimetric Vacuum Emissometer, shown in Figure 5.1, and the problems encountered in operating the system. The sample, heat flow sensor, and copper block made up the sample holder. The sample holder was mounted on a large vacuum flange, which contained much of the instrumentation and wiring for the system. The flange was attached to the outer of two chambers, which encloses the sample. The final component of the system was the vacuum system itself.

The sample holder was a 3 x 3 x 3/4 inch copper block. Copper was chosen because its excellent heat conductance would provide uniform

41
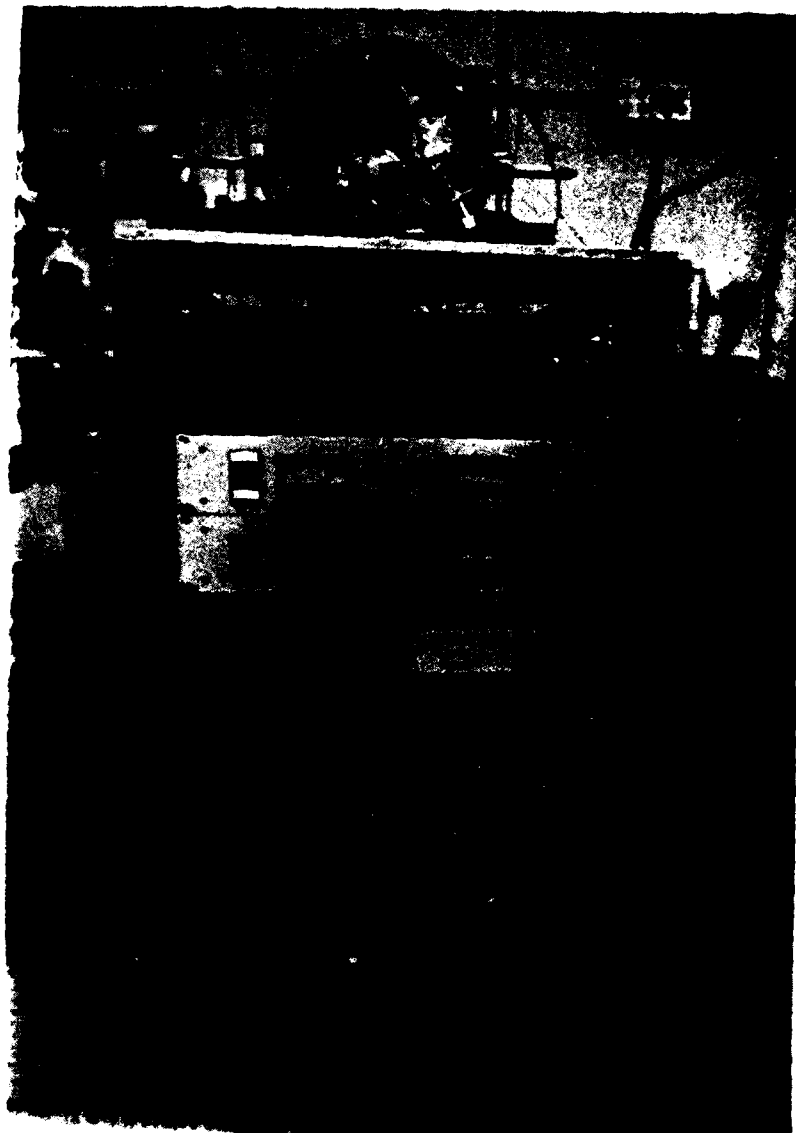


Figure 5.1.  Front view of the CVE; from top to bottom, sample
chamber, thermocouple selector and readout, ion
gauge readout, thermocouple vacuum gauge readout,
power supply readout, and power supply.

sample heating.  Centered on one of the large faces was a 2 x 2 inch recess milled to a depth of 0.1 inch for the sample.  This area held the heat flow sensor, a wafer thin square of Kapton with four thin wires attached at the bottom.  A small groove was also milled for these wires.  Flush on the surface of the milled area were mounted four thermocouples with their associated wires emerging from the back of the copper block.  The sample and heat flow sensor were held in place by four small aluminum clamps screwed down onto the four corners of the sample.  Teflon pieces about 1/4 inch square were used to separate and insulate the sample from the aluminum.  Four cartridge heaters inserted in the top of the copper block provided the heat source.  The copper block itself was mounted on the vacuum flange by two 1/8 inch stainless steel standoffs and a section of 1/4 inch copper tubing.  The sample holder in shown in Figure 5.2.

The vacuum flange served as the door to the system and also the interface from the sample to the outer world.  The flange contains three sets of vacuum feedthroughs for wires of the thermocouples, thermopile, and the heaters, all of which can be seen in Figure 5.3.  The flange also supported parts for two thermocouple vacuum gauges and a  port for an ion vacuum guage.  The air admittance valve, necessary to return the system to atmospheric pressure, was also mounted here.  Twelve bolts and a 12 inch diameter, 1/4 inch thick O-ring provided the necessary vacuum seal for the outer chamber.

Figure 5.2.   CVE sample holder with sample.
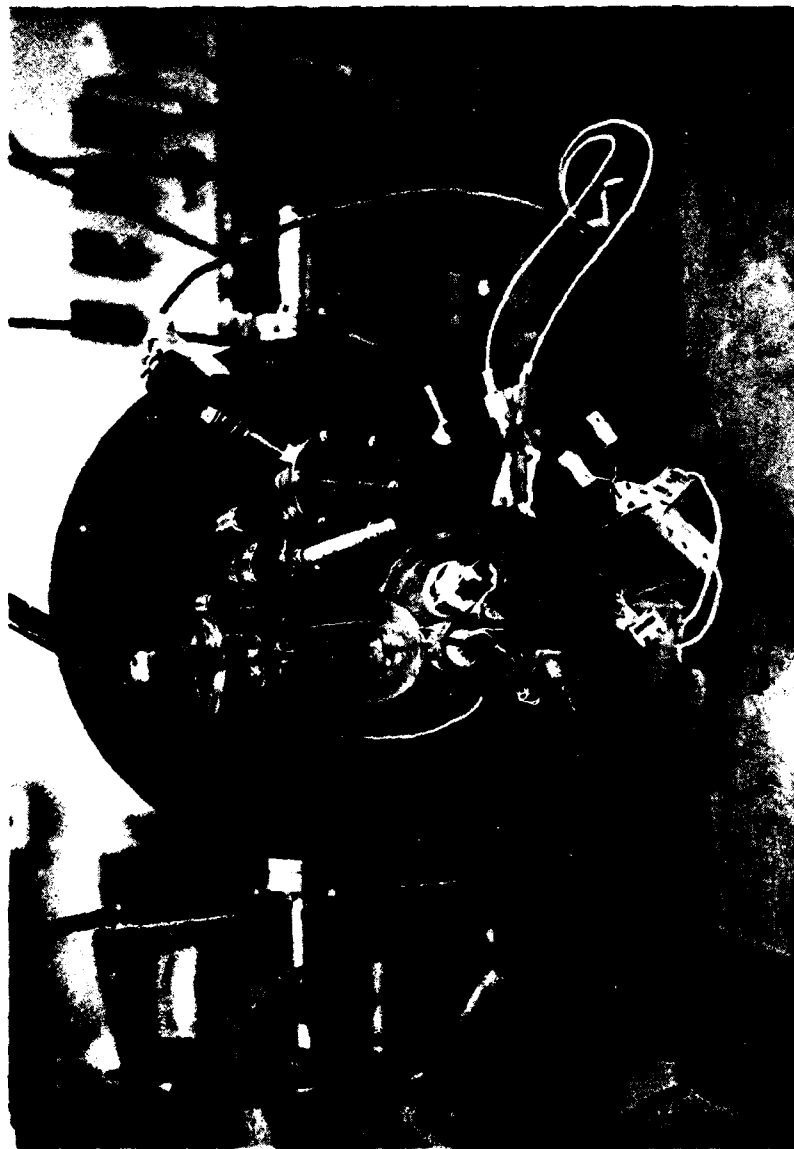
Figure 5.3. Exterior of the vacuum flange of the CVE.

The sample is held inside a double enclosure, an outer stainless steel cylinder and the inner sample cavity. The steel cylinder is approximately 24 inches long and ten inches in diameter. It is mounted horizontally and connects to the diffusion pump underneath through a high vacuum valuve. One end of the cylinder is closed off while the other end has a flange welded to it to mate with the flange previously described. On either side of the flange and of the cylinder are two ports, through which liquid nitrogen is pumped into the sample cavity.

The sample cavity is made of 1/4 inch copper tubing wound and soldered together into a cylinder 6 inches in diameter and 16 inches long. Both ends of the cylinder are capped by 1/8 inch thick copper plates soldered in place. In one end, a square opening was cut in the plate just large enough to accommodate the sample holder without actually touching a side, see Figure 5.4. The two ends of the copper tubing exit the steel cylinder through the two side ports. Liquid nitrogen pumped through the tubing cools the cavity to 77 K, cold enough to eliminate virtually all thermal radiation from the cavity walls. The interior of the cavity has been painted with 3M's Nextel Black Velvet Coating. This paint has a measured absorptance of 95%, which reduces the reflected thermal radiation of the sample to a negligible amount. The sample cavity is supported only by the two connections at the liquid nitrogen ports and by a small acrylic spacer which limits heat flow to the sample cavity, diffusion vacuum pump, two valves, three thermocouple vacuum gauges, and one ion vacuum gauge. The mechanical pump is connected by the first valve to either the

Figure 5.4.  Interior of CVE cavity, with cylinder of copper
tubing and vacuum ports for liquid nitrogen.

sample chamber or the backing side of the diffusion pump. Initially, the mechanical pump is used to evacuate the sample chamber. Then the mechanical pump is connected to the diffusion pump and through the high vacuum valve, the diffusion pump evacuates the sample chamber to high vacuum. The thermocouple gauges monitor the performance of the mechanical pump in different locations while the ion gauge measures the high vacuum developed by the diffusion pump.

Vacuum problems were the major difficulties encountered on this project. Vacuum problems were finally resolved into two categories, actual leaks and outgassing. Leaks were found in virtually every joint. An attempt to provide rapid cooling of the sample by a cooling water line was abandoned because of the inability to overcome vacuum problems. Another major problem was the interface between the sample cavity tubing and the vacuum ports of the steel cylinder. O-rings were used to provide a vacuum seal but under the thermal stress of cycling from room to liquid nitrogen temperatures, the O-rings soon disintegrated. The O-rings were finally eliminated by making a direct soldered connection, but even this leaked under high vacuum when cooled.

Despite meticulous care in tracking down possible leak sources, the obtainable vacuum was not sufficient to suppress heat loss. Outgassing was then considered. The diffusion pump was left on continuously for several weeks to allow it to clean itself and a small improvement was noted. All unnecessary items were removed from the cavity and the remaining items were cleaned with acetone. This did not help. Finally, the inner painted surface of the sample cavity was targeted as the

culprit. Before cooling by liquid nitrogen, hot tap water was run overnight through the tubing. The temperature of the water was approximately 60 C. The vacuum improved by two orders of magnitude. Unfortunately, every time the sample was changed, the paint re-adsorbed enough gas to require degassing by hot water. This made the emittance measurement a two-day process, one to outgass and prepare the system, and a second for the actual measurement.

Another problem encountered only twice was the formation of a film of foreign matter on the sample surface. This was due to an accidental interruption of the cooling water for the diffusion pump, causing the diffusion pump oil to overheat and contaminate the sample. Fortunately, this was discovered during the initial calibration runs. Afterwards, the samples were measured before and after the emissometer runs in an intergrating sphere reflectometer and the Perkin-Elmer 137 infrared reflectometer to reveal any surface changes. No changes were noted after this procedure was instituted.

The electronics were another source of problems. The basis of the emissometer was the heat flow sensor, a set of thermocouples. Its microvolt output was difficult to measure and several instruments were tried before one was found with enough sensitivity and stability. Chromel-alumel type thermocouples were employed to measure the sample's temperature and were read by an Omega Engineering 199 digital thermometer readout. The thermocouple feedthrough were another major leak source and the wires themselves had to be protected from the heat source, as was found when some shorted after their insulation melted. Several

ion vacuum tubes developed defects or vacuum leaks and had to be replaced.

The final major problem faced was the power source for the cartridge heaters. First, a simple AC power supply was used but was discarded because it was thought to have insufficient power. Next, a commercial temperature controller was used. The temperature controller was a power supply with a thermocouple feedback and logic circuits to maintain the set temperature. This also appeared to have insufficient power until it was found that the copper sample holder was in contact with the sample cavity, a massive heat sink. Once the contact was eliminated, the power problem vanished but another problem appeared. The temperature controller oscillated continuously, and even though the osciallations could be damped, they were apparent on a large scale several hours after starting a run. Since thermal equilibrium was required, the temperature controller was inadequate. The original power supply was returned to the system, and with the thermal contact eliminated, it too had enough power. Although it took 2 to 3 hours to reach thermal equilibrium, this power supply allowed the sample to approach thermal equilibrium in a much more predictable fashion.

The CVE has been described in a qualitative manner in this chapter. The steps taken to reduce unwanted heat flow were detailed. Based on these steps, we have claimed that Equation 5.1 is reduced to Equation 5.2, which allows us to compute emittance directly. A more thorough explanation of the CVE operating procedures is contained in Applendix A. In Chapter 5, Eq. 5.1 is evaluated in a quantitative manner to determine the accuracy of the CVE.

CHAPTER 6

CALIBRATION OF THE CALORIMETRIC
VACUUM EMISSOMETER

This chapter is divided into two parts.  First, the heat loss

balance described by Equation 5.1 is examined in close detail, both

for the emittance calculation and for appropriate error limits.  Second,

to calibrate our instrument against the results of others, two sets of

measurements will be compared with values published in the "Thermo-

physical Properties of Matter, Volume 7, Thermal Radiative Properties",

1970, edited by Touloukian and DeWitt.  This comparison will show that

our values compare favorably with measurements made by others.

## Calculation of Emittance and
## Relative Error

Equation 5.1 is the basis of this section, and so is repeated

here.

$$Q(total) = Q(conv) + Q(cond) + Q(sc) + Q(a) + Q(h) - Q(r) \quad 5.1)$$

Under thermal equilibrium, Q(total) is zero.  We have previously implied

that first four terms on the right are also zero, so that Q(h), the

conductive heat flow into the sample equals Q(r), the heat energy

radiated from the sample.  We will now examine the magnitude of each

term on the right side of Equation 5.1.

The conductive heat flow can be broken into two parts.  At

higher pressures, heat can be transported by both air conduction and

convection. However, at the operating pressures of the CVE, the distinction is difficult. We will separate them anyway, simply to distinguish between two possible heat transport mechanisms.

Q(conv) is described here as the thermal energy transfer between two surfaces by molecules striking one surface and gaining thermal energy, then colliding with more molecules, with the energy being transferred in each collision until the thermal energy from the first surface finally arrives at the second surface. It is the multiple collisions of air molecules that differentiates this form of heat transfer from conduction. If the pressure is too low to give multiple collisions a finite probability over the dimension of the system, Q(conv) is effectively zero.

A molecule's mean free path is the statistical average distance it travels between collisions. When the mean free path is significantly larger than any interior dimension of the chamber, it is obvious that molecules are traveling directly from surface to surface with no intervening collisions. Kittel, in his book, "Thermal Physics" (1969), defines mean free path as

$$\ell = \frac{1}{\pi d^2 n} \tag{6.1}$$

where d is the molecular radius and n is the Loschmidt number 2.69 x 10^19 atoms per cubic centimeter at 760 mm of mercury and 0 C. Assuming 5 x 10^-6 Torr, the mean free path is approximately 5 meters. Since the largest interior dimension is approximately 0.5 meters, it is obvious that few collisions are occurring. It follows that the heat

transfer, Q(conv), based on multiple collisions, is effectively zero (Kittel, 1969).

Q(cond) is the heat transfer by molecule carrying thermal energy directly from surface-to-surface without multiple collisions. The energy transfer per molecule is

$$1/2 \ K \ [T(hot) - T(cold)] \tag{6.2}$$

where the quantity in parentheses is the temperature differential between the hot and cold surfaces and K is the Boltzmann constant. To obtain the total heat flow, the number of molecules striking the sample per second must be obtained. This can be computed from the pressure.

Pressure can be defined as the momentum change per molecule times the number of collisions per unit time per unit area. We will again use $5 \times 10^{-6}$ Torr and so only need to compute the momentum change per molecule to obtain the required number of collisions per unit time per unit area.

The momentum change of a molecule hitting a wall and rebounding in an elastic collision is simply twice the momentum of the molecule in the direction normal to the surface. Since the atmosphere is basically 80% nitrogen and 20% oxygen, we assume that an average molecule's mass is that of air, is 28.8 atomic mass units. The molecule's velocity component perpendicular to the suface can be obtained by the following equation, again from Kittel.

$$\text{average molecular velocity} = \left(\frac{2KT}{\pi m}\right)^{\frac{1}{2}}$$

where K is the Boltzmann constant, T the temperature, and M the mass.
With the mass and velocity now computed, the momentum change is also
known, and the average number of collisions per unit time per unit area
can be calculated. One atmosphere of pressure is $1.013 \times 10^{-6}$ dynes per
square centimeter, which when scaled for our vacuum and then divided
by the average momentum change per molecule gives the number of col-
lisions per unit area per unit time. For the temperatures between 50 C to
150 C, the numbers are $2.86 \times 10^{-15}$ to $2.50 \times 10^{-15}$ collisions per
second per square centimeter. These numbers times the energy transfer
per molecule, Equation 6.2, provide the total Q(cond), 1.25 to 1.54 x
$10^{-4}$ Watts for 50 C to 160 C. These values of Q(cond), when compared
to a material with the extremely low emittance of 1% provide a relative
error of less than 1%, which will be shown to be much less than our
measurable accuracy. Therefore, Q(cond) is effectively zero.

Q(sc) is the thermal energy transfer due to conduction of the
supports. Since all the thermal energy entering the sample goes through
the heat flow sensor, this is assumed to be neglible. There may be a
small unmeasured heat flow through the Teflon spacers and clamps, but
since Teflon is an excellent thermal insulator, it is assumed to be
unimportant.

Q(a) is the radiant thermal energy absorbed by the sample in the
CVE. This term actually consists of two parts, thermal radiation from
the walls and the sample's own radiation reflected from the walls. The
thermal radiation arriving at the sample from the walls of the cavity is

$$Q(a-rad) = \sigma T^4 F_{w \to s} A_w \tag{6.4}$$

where $\sigma$ is the Stefan-Boltzmann constant, T the temperature of the walls, $F_{w \to s}$ the shape factor that accounts for the geometry and the emittance of the surfaces involved, and $Q_w$ the area of the walls. The product of the sahpe factor and the area is equal to the product of the sample's shape factor and its area, i.e.,

$$F_{w \to s} A_w = F_{s \to w} A_s \tag{6.5}$$

The sample's shape factor can be found in several books on thermal radiation; the one we use was published in an ANSI-ASTM article

$$F_{s \to w} = \frac{1}{1/\epsilon_1 + A_1/A_2 \ (\epsilon_2 - 1)} \tag{6.6}$$

where $\epsilon_1$ is the emittance of the sample, $A_1$, the sample area, $\epsilon_2$, the walls emittance, and $A_2$, the area of the walls. The ratio of the areas $A_1/A_2$ is 0.01 and the emittance of the walls, painted with Nextel Black Velvet , is 0.95 (measured on the Perkin-Elmer 137). Thus, the shape factor is simply the emittance of the sample. Q(a-rad) is then merely the ratio of the wall temperature to the sample temperature, all to the fourth power. To minimize Q(a-rad), the walls are cooled with liquid nitrogen to 77 K. Even at the lowest sample temperature of 50 C, 323 K, the error is only 0.3%.

Q(a-refl) is the thermal energy radiated by the sample and reflected by the walls back to the sample. Since the walls are coated with the highly absorbant paint, only a single reflection need be considered; with each reflection, only 5% of the beam's energy remains. The walls' painted surfaces are very rough, and so radiation incident at angles far from normal gets trapped. Normally incident radiation

that is reflected off the back surface is also reflected into a pro-
jected solid angle of $\pi$ steradians, and the amount in the small solid
angle that does return to the sample is so small that it can be
neglected.

The remaining terms of Equation 5.1 are the ones to be deter-
mined. Q(h) is the heat flow leaving the surface of the thermopile.
It is measured by the thermopile, which has an output in microvolts.
A simple calculation transforms the voltage into radiated power. This
heat flow first crosses a thin coating of vacuum grease and then enters
the sample. We assume the thermal resistance across the vacuum grease
to be negligible, so that all the power leaving the thermopile enters
the sample. The power entering the sample must equal the power being
radiated by the sample, Q(r), which is given by the Stefan-Boltzmann Law,

$$Q(n) = Q(e) = \epsilon \sigma T^4 \qquad (6.7)$$

Equation 5.1 has now been completely quantified. Based on the
discussion in this chapter, the total hemispherical emittance as
determined by the CVE is

$$\epsilon = \frac{CVA + 1.25 \times 10^{-4} (323/T)^{\frac{1}{2}} (T-77)/246}{A\sigma(T^4 - 77^4)} \qquad (6.8)$$

where C is the microvolt-watts conversion factor of the thermopile,
V is the voltage, A is the area of the sample, 25.8 sq. cm., T is the
temperature, and $\sigma$ is the Stefan-Boltzmann constant. Note that the
emittance is a function of temperature and voltage. Although two

factors in this equation have been determined to be negligible, they have been included to ensure that the error calculation *is* accurate.

The relative error of the emittance measurement is the total differential of emittance divided by the emittance. The total differential of the emittance is

$$|\delta\epsilon| = \frac{\{CA\delta V + (\frac{1}{2} \cdot 1.25 \times 10^{-4} (323/T^3)^{\frac{1}{2}} (T-77)/246}{A^2 \sigma^2 (T^4 - 77^4)^2}$$

$$+ \frac{125 \times 10^{-4} (323/T)/246)\}\delta T}{A^2 \sigma^2 (T^4 - 77^4)^2} \tag{6.9}$$

$$+ \frac{\{CVA + 1.25 \times 10^{-4} (323)/T)(T-77)/246\} \ 4A\sigma T^3 \ \delta T}{A^2 \sigma^2 (T^4 - 77^4)^2}$$

Equations 6.8 and 6.9 were the equations used in the determining the emittance and the relative error in all measurements. The relative error varied inversely with the emittance, with emittance values from 0.02 to 0.38 the relative error varied from 11% to 2.8%. This magnitude of error is comparable to other published values. For example, the error limits reported in the "Thermophysical Properties of Matter", when given at all, range from 2% to 20% (Touloukian and DeWitt, 1970).

Based on the above analysis, the CVE is at least as accurate as other calorimeters used to measure emittance. This discussion has all been theoretical, however; only the actual performance of the CVE on known test materials would confirm its accuracy. This is the subject of the next section.

## CVE Performance Data

The standard for comparison with our CVE results was the data published in the "Thermophysical Properties of Matter, Volume 7, Thermal Radiative Properties". Aluminum and nickel were chosen as test samples because of the ease in obtaining samples and because many data sets were available on these two materials. The results are shown on the following pages in Figure 6.1 and 6.2, and in Table 6.1 and 6.2. The tables are of CVE data and the graphs show placement of CVE data relative to measurements by others.

The aluminum emittances, as determined by the CVE at 50 C, 100 C, and 150 C, appears to run below other measurements, generally, and to have a scattering of values especially at the 50 C temperature. Two explanations of the lower emittance could be that our samples were smoother than others' samples and that our vacuum was better, both of which are substantiated by the description of their measurements. More substantiation will come in the next chapter when a comparison will be made with the Bennett normal reflectance data. The scattering is harder to explain, except that the CVE vacuum is usually one order of magnitude worse by the end of the last measurement of each emittance at the lower temperature. Also, the aluminum samples varied from new to several years old, which also could explain the deviations.

The nickel CVE data was much more consistent. All three nickel samples produced very similar results. Also, the data from the reference cited was also more consistent for nickel than for aluminum. As shown on the nickel graph, the CVE data appears to fall very close to several other measurements.

The results described in this chapter enabled us to state that the CVE produced accurate results in the measurement of total hemispherical emittance. The CVE then qualified as a standard against which the optically derived emittance could be compared. The next chapter will describe the operation of the CVE, though, before the actual comparison of the optical and calorimetric data is presented.

Table 6.1.  Total Hemispherical Emittance Data for Aluminum as Determined
by the Calorimetric Method (CVE).

| Temperature | Sample #1 | Sample #2 | Sample #3 | Mean |
|---|---|---|---|---|
| 50 C | 0.0120 | 0.0129 | 0.0150 | 0.0133 |
| 100 C | 0.0129 | 0.0124 | 0.0124 | 0.0126 |
| 150 C | 0.0140 | 0.0136 | 0.0131 | 0.0136 |

Table 6.2.  Total Hemispherical Emittance Data for Nickel as Determined
by the Calorimetric Method (CVE).

| Temperature | Sampel #1 | Sample #2 | Sample #3 | Mean |
|---|---|---|---|---|
| 50 C | 0.0586 | 0.0579 | 0.0585 | 0.0583 |
| 100 C | 0.0668 | 0.0668 | 0.0668 | 0.0668 |
| 150 C | 0.0810 | 0.0802 | 0.0794 | 0.0802 |
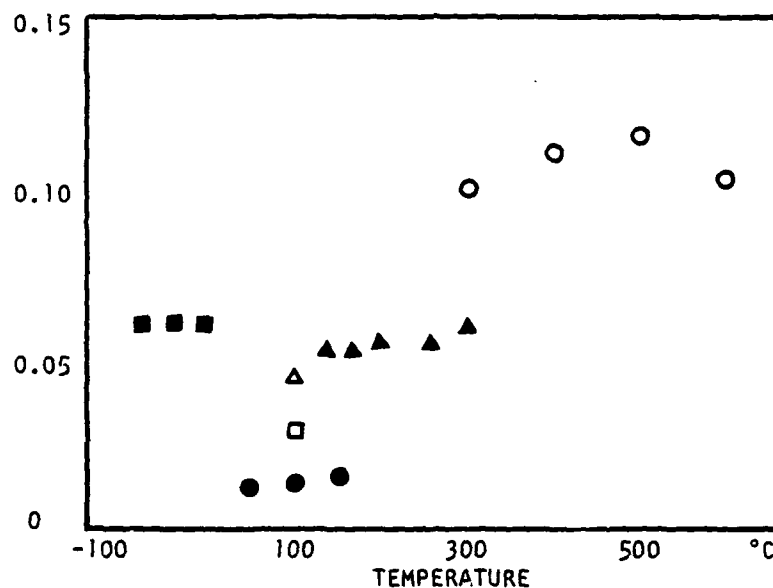
Figure 6.1. Total hemispherical emittance of aluminum as a
function of temperature as reported by different
measurements.

● CVE data

○ Calculated from spectral data, #1*

■ Plate 0.2 inch thick, hand polished, vacuum $10^{-3}$ Torr, #31*

□ 99.99 pure; prefinished with 600 grit aluminum oxide powder
on felt, electropolished, vacuum $10^{-5}$ Torr, #35*

△ Same as above except bombarded with hydrogen ions (9.840 x
$10^{20}$ ions/cm$^2$), #38

▲ Hollow sphere; polished to approx. 5 microns then rinsed
with distilled water and alcohol, dried in nitrogen; measured
in vacuum, #40

*Data from Thermophysical Properties of Matter, numbers are data
set nos. (Touloukian and DeWitt, 1970).
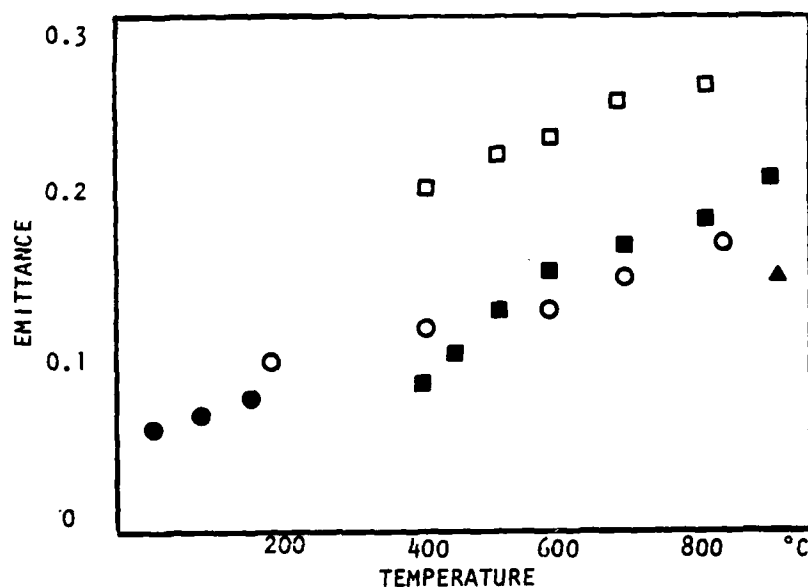
Figure 6.2.   Total hemispherical emittance of nickel as a function
of temperature as reported by different measurements.

● CVE data

□ Plated on aluminum; buffed; vacuum $10^{-7}$ Torr, #2*

○ Foil 0.0015 in. thick, vacuum $10^{-6}$ Torr, #3*

■ Foil $10^{-5}$ in. thick, solvent cleaned, $10^{-6}$ Torr, #10*

▲ Foil 0.0005 in. thick, solvent cleaned, $10^{-6}$ Torr, #11*

*Data from Thermophysical Properties of Matter, numbers are
data set nos. (Touloukian and DeWitt, 1970).

CHAPTER 7

RESULTS

This chapter contains the measurements of total hemispherical emittance $\epsilon$, and total normal emittance $\epsilon_n$. The ratios of these measured quantities, $\epsilon/\epsilon_n$ are also compared with the ratios derived from the Fresnel equations. This data is presented in Tables 7.1 and 7.2. Table 7.3 again presents the ratio, $\epsilon/\epsilon_n$, but this time as a ratio of the measured quantity versus the predicted quantity. Table 7.4 shows the relative error in total radiative loss from using NNISR to derive total normal emittance, and then the Fresnel ratio to obtain total hemispherical emittance instead of using the calorimetrically measured total hemispherical emittance. Figures 7.1 through 7.13 show the individual samples total hemispherical emittance and the agreement of the ratio $\epsilon/\epsilon_n$ measured with the Fresnel ratio.

Tables 7.1 and 7.2 contain many elements and so will be explained in detail. The two tables separate the measurements made for calibration of the CVE from the actual research done on molybdenum thin films. Under each material is first listed the measured total normal emittance as derived from NNISR. In the case of aluminum, an additional total normal emittance is listed, which was derived from the Bennett data (Bennett, Silver and Ashley, 1963). Following the total normal emittances, in all cases, are the total hemispherical emittances, first as derived from the NNISR and the Fresnel relations, and then,

62

as determined by the calorimetric method.  Then are listed the ratios

of total hemispherical emittance to total normal emittance.  The first

ratio shown is based on the measured quantitites listed above, i.e.,

the CVE determined total hemispherical emittance and the total normal

emittance derived from NNISR measured on the Perkin-Elmer 137.  The

second ratio is based on the Fresnel expressions.  The value listed as

the Fresnel ratio was obtained from Figure 4.1, a graph of the ratio as

a function of the normal emittance, using the measured total normal

emittance as the input.

The four molybdenum samples vary only in annealing time after

deposition.  The Super Molybdenum sample was annealed at 1000 C for 10

minutes.  Samples #1 and #2 were annealed at 700 C  for 3 minutes and 1

minute, respectively.  Black Molybdenum #3 was as-deposited, i.e., no

anneal.  The effect of annealing will be discussed in Chapter 8.

Table 7.1 Total Hemispherical Emittance $\varepsilon$, Total Normal Emittance $\varepsilon_n$, and a Comparison of Ratios $\varepsilon/\varepsilon_n$, as Measured and as Predicted Using the Fresnel Equations for Aluminum and Nickel

| | Temperature | 50 C | 100 C | 150C |
|---|---|---|---|---|
| **ALUMINUM** | | | | |
| $\varepsilon_n$ | | 0.020 | 0.021 | 0.023 |
| $\varepsilon_n$ | (Bennett) | | | 0.019 |
| $\varepsilon$ | (Optical) | 0.026 | 0.027 | 0.030 |
| $\varepsilon$ | (Calorimetric) | 0.013 | 0.013 | 0.014 |
| RATIO $\varepsilon/\varepsilon_n$ | | | | |
| | CVE/PE137 | 0.65 | 0.62 | 0.61 |
| | FRESNEL | 1.30 | 1.30 | 1.30 |
| **NICKEL** | | | | |
| $\varepsilon_n$ | | 0.59 | 0.61 | 0.61 |
| $\varepsilon$ | (Optical) | 0.71 | 0.75 | 0.74 |
| $\varepsilon$ | (Calorimetric) | 0.58 | 0.67 | 0.80 |
| RATIO $\varepsilon/\varepsilon_n$ | | | | |
| | CVE/PE137 | 0.98 | 1.10 | 1.31 |
| | FRESNEL | 1.23 | 1.23 | 1.22 |

Table 7.2. Total Hemispherical Emittance $\epsilon$, Total Normal Emittance $\epsilon_n$, and a Comparison of Ratios $\epsilon/\epsilon_n$, as Measured and as Predicted Using the Fresnel Equations for Super Molybdenum, and Black Molybdenum Samples #1, #2, and #3.

| Temperature | 50 C | 100 C | 150 C |
|---|---|---|---|
| **SUPER MOLYBDENUM** | | | |
| $\epsilon_n$ | 0.020 | 0.021 | 0.023 |
| $\epsilon$ (Optical) | 0.250 | 0.026 | 0.029 |
| $\epsilon$ (Calorimetric) | 0.040 | 0.043 | 0.050 |
| RATIO | | | |
| CVE/PE137 | 2.00 | 2.05 | 2.17 |
| FRESNEL | 1.25 | 1.25 | 1.24 |
| **BLACK MOLYBDENUM #1** | | | |
| $\epsilon_n$ | 0.076 | 0.072 | 0.074 |
| $\epsilon$ (Optical) | 0.091 | 0.086 | 0.088 |
| $\epsilon$ (Calorimetric) | 0.103 | 0.110 | 0.124 |
| RATIO | | | |
| CVE/PE137 | 1.35 | 1.48 | 1.67 |
| FRESNEL | 1.20 | 1.20 | 1.19 |
| **BLACK MOLYBDENUM #2** | | | |
| $\epsilon_n$ | 0.107 | 0.108 | 0.111 |
| $\epsilon$ (Optical) | 0.125 | 0.126 | 0.129 |
| $\epsilon$ (Calorimetric) | 0.143 | 0.149 | 0.171 |
| RATIO | | | |
| CVE/PE137 | 1.34 | 1.38 | 1.54 |
| FRESNEL | 1.17 | 1.17 | 1.16 |

Table 7.2.  Continued

|  | Temperature | 50 C | 100 C | 150 C |
|---|---|---|---|---|
| BLACK MOLYBDENUM #3 |  |  |  |  |
| $\varepsilon_n$ |  | 0.233 | 0.243 | 0.273 |
| $\varepsilon$ | (Optical) | 0.251 | 0.257 | 0.284 |
| $\varepsilon$ | (Calorimetric) | 0.307 | 0.345 | 0.377 |
| RATIO |  |  |  |  |
| CVE/PE137 |  | 1.32 | 1.42 | 1.38 |
| FRESNEL |  | 1.08 | 1.06 | 1.04 |

Table 7.3. Ratio of Measured to Predicted Ratio of Total
Hemispherical Emittance to Total Normal Emittance, Measured
by the CVE and Perkin-Elmer 137 Spectrometer and Predicted
by the Fresnel Equations.

| Temperature | 50 C | 100 C | 105C |
|---|---|---|---|
| ALUMINUM | 0.50 | 0.48 | 0.47 |
| W/Specular Assumption | 0.98 | 0.98 | 1.05 |
| NICKEL | 0.80 | 0.89 | 1.07 |
| SUPER MOLYBDENUM | 1.60 | 1.64 | 1.75 |
| BLACK MOLYBDENUM #1 | 1.13 | 1.23 | 1.40 |
| BLACK MOLYBDENUM #2 | 1.14 | 1.18 | 1.33 |
| BLACK MOLYBDENUM #3 | 1.22 | 1.34 | 1.33 |

Table 7.4.  Relative Error in Total Radiative Loss from Using Optical
Means of Driving Total Hemispherical Emittance as Compared
to the Calorimetric Method.

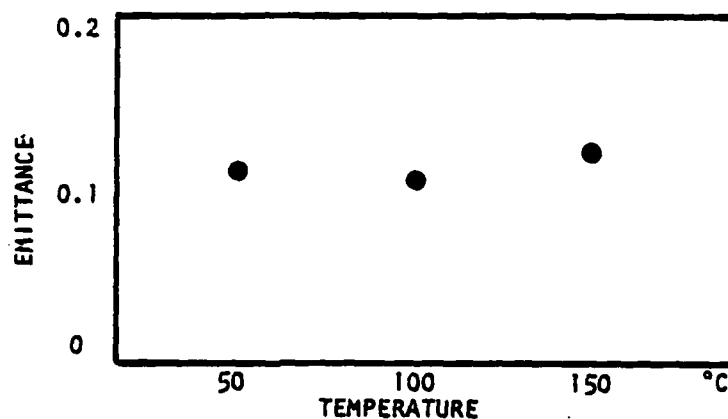| Temperature | 50 C | 100 C | 105 C |
|---|---|---|---|
| ALUMINUM | 54% | 62% | 64% |
| w/1% Specular Assumption (See Chapter 8) | 02% | 02% | 05% |
| NICKEL | 25% | 12% | 7% |
| SUPER MOLYBDENUM | 37% | 29% | 43% |
| BLACK MOLYBDENUM #1 | 11% | 21% | 29% |
| BLACK MOLYBDENUM #2 | 12% | 15% | 25% |
| BLACK MOLYBDENUM #3 | 18% | 25% | 25% |

Figure 7.1.   Total hemispherical emittance of aluminum as determined by the calorimetric method (CVE).
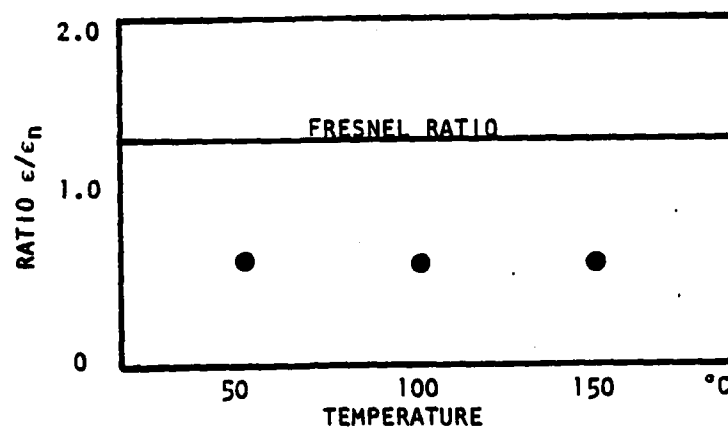


Figure 7.2.   Measured and predicted ratios of total hemispherical emittance to total normal emittance for aluminum.
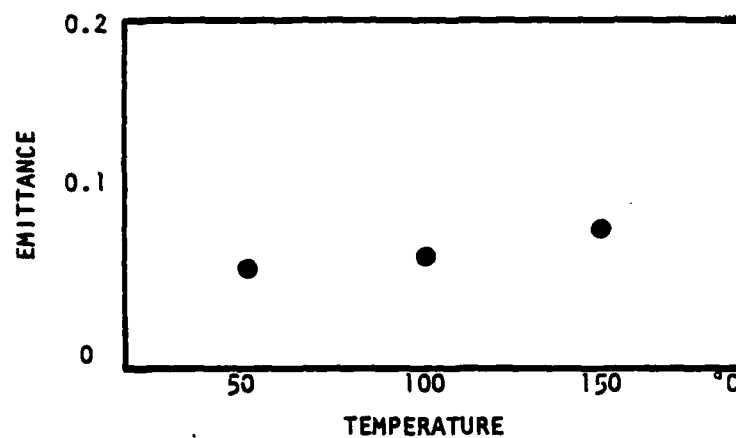
Figure 7.3. Total hemispherical emittance of nickel as determined by the calorimetric method (CVE).
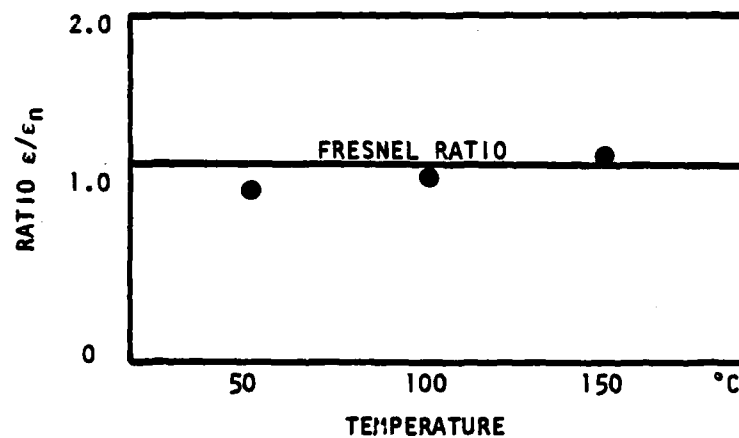


Figure 7.4. Measured and predicted ratios of total hemispherical emittance to total normal emittance for nickel.

Figure 7.5. Total hemispherical emittance of "Super Molybdenum"
and "Black Molybdenum", samples #1, #2, and #3,
as determined by the calorimetric method (CVE).

● Super Molybdenum

○ Black Molybdenum #1

□ Black Molybdenum #2

■ Black Molybdenum #2

Figure 7.6.  Total hemispherical emittance of "Super Molybdenum"
as determined by the calorimetric method (CVE).



Figure 7.7.  Measured and predicted ratios of total hemispherical
emittance to total normal emittance for "Super
Molybdenum".

Figure 7.8.  Total hemispherical emittance of "Black Molybdenum"
#1 as determined by the calorimetric method (CVE).



Figure 7.9.  Measured and predicted ratios fo total hemi-
spherical emittance to total normal emittance
for "Black Molybdenum" #1.

Figure 7.10.  Total hemispherical emittance of "Black Molybdenum"
#2 as determined by the calorimetric method (CVE).



Figure 7.11.  Measured and predicted ratios of total hemi-
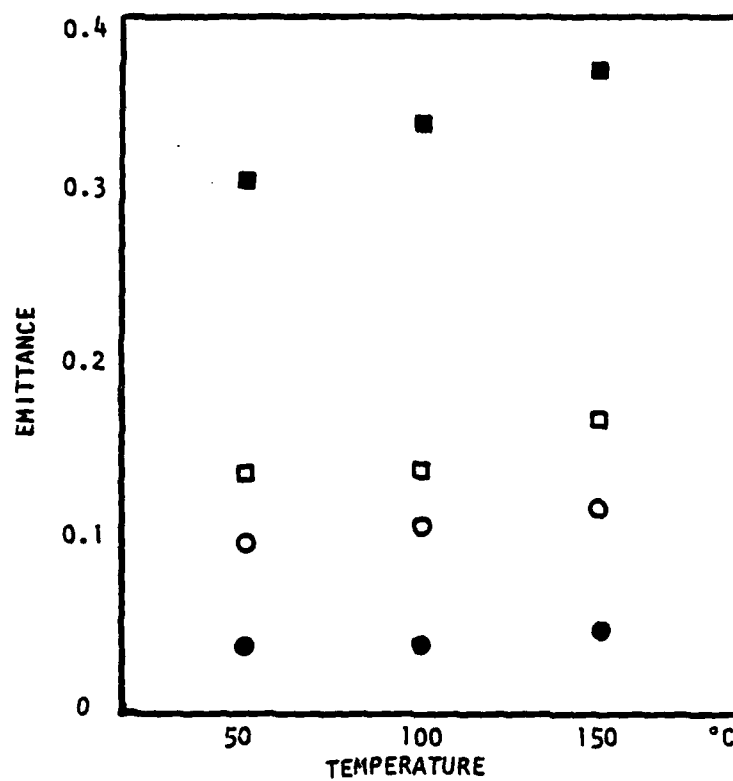spherical emittance to total normal emittance
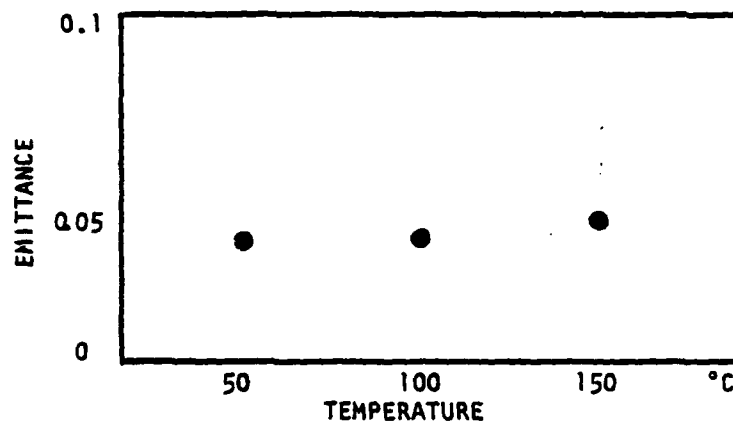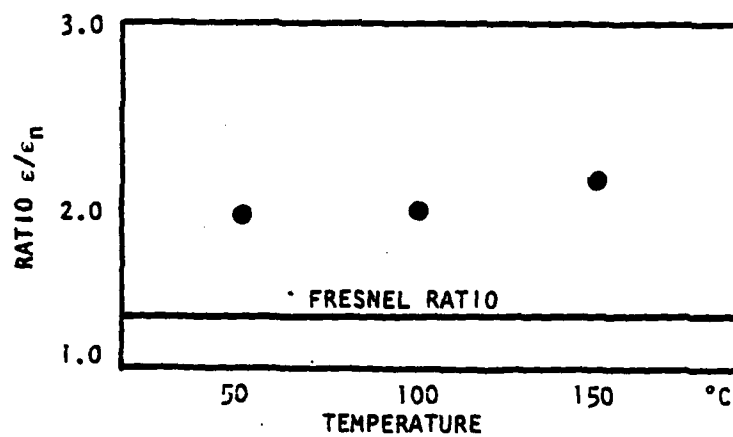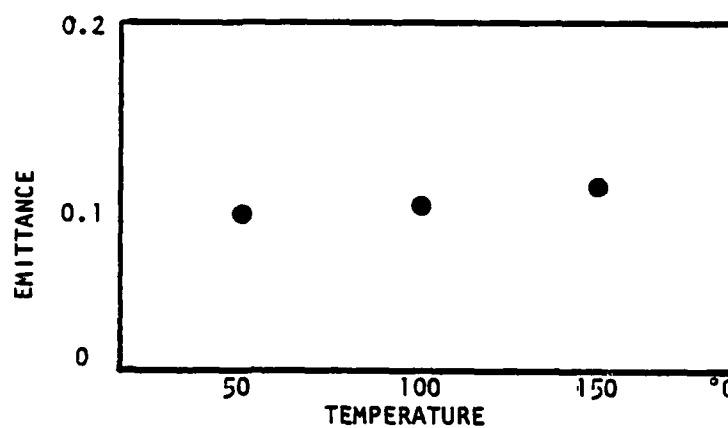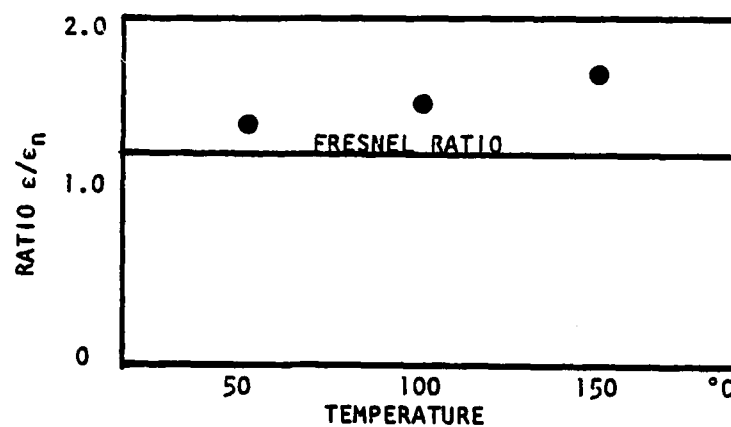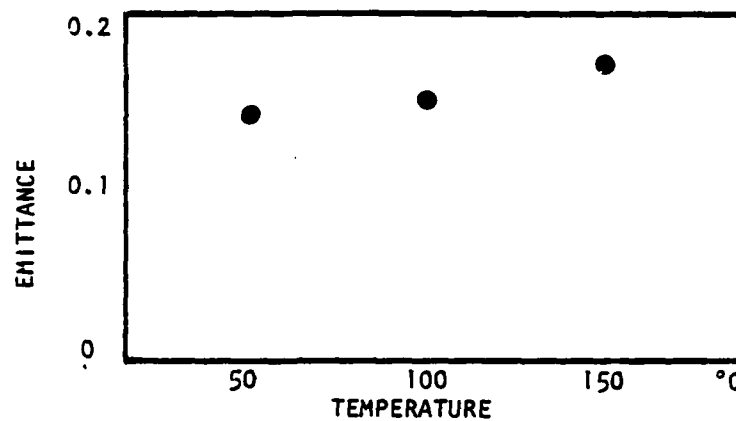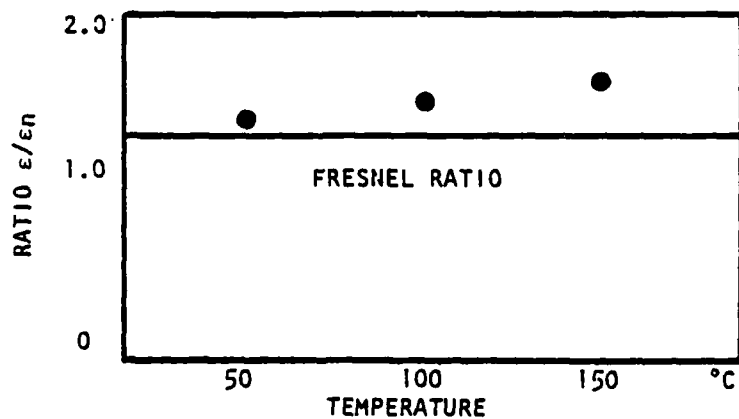for "Black Molybdenum" #2.
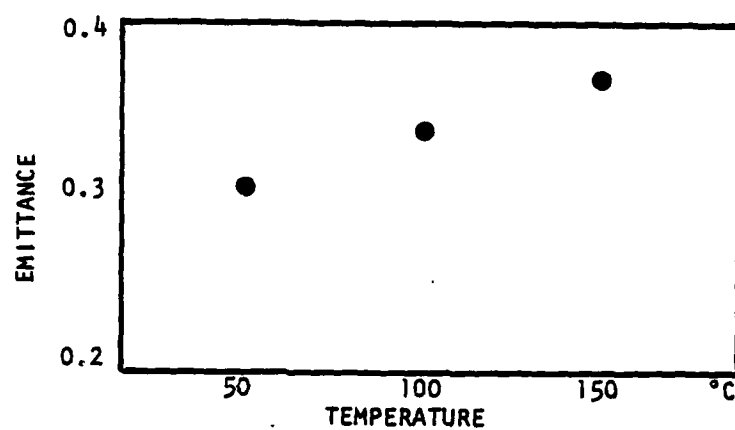
Figure 7.12. Total hemispherical emittance of "Black Molybdenum" #3 as determined by the calorimetric method (CVE).
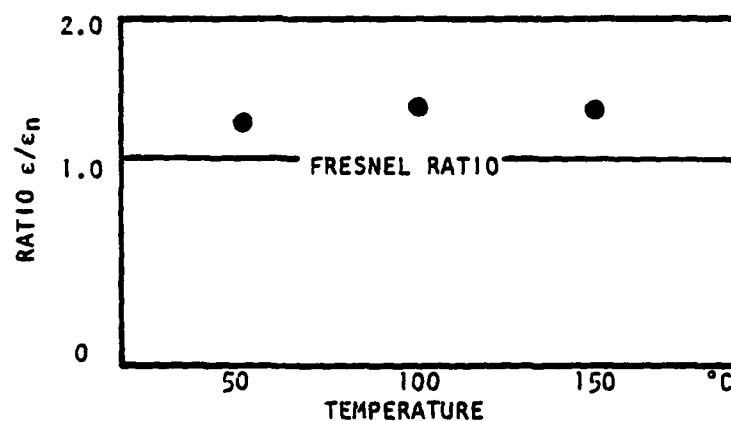


Figure 7.13. Measured and predicted ratios of total hemispherical emittance to total normal emittance for "Black Molybdenum" #3.

CHAPTER 8

DISCUSSION

This chapter deals with the primary purpose of this thesis, a comparison of optical method of determining total hemispherical emittance with the calorimetric method. The calorimetric means was shown in Chapter 6 to be an accurate, direct measurement of the total radiative loss of a material. The optical means of deriving total hemispherical emittance from a NNISR measurement was shown in Chapter 4 to require four assumptions and approximations, which cast doubt on its accuracy. These assumptions and approximations will now be evaluated for their effect on the calculated emittance. This will provide a tool with which the results listed in Chapter 7 can be analyzed.

The first optical measurement assumption is discussed in Chapter 4 was specularity. The optical method is based on a near normal incidence, spectral reflectance measurement. This quantity can be converted to a directional spectral emittance by subtraction from one. We assume the measured quantity is the directional hemispherical spectral reflectance. This is true only if all the reflected radiation is measured by the detector. The detector, however, measures not all the reflected radiation from the surface but only that reflected in a small solid angle around the angle of reflection suggested by geometric ray optics. All the reflected energy would be measured only if the sample

76

was perfectly specular, but, since there are not perfectly specular
materials, the measured reflectance is less than the actual directional
hemispherical spectral reflectance and the calculated directional
spectral emittance is too large. Thus, the specular assumption leads
to an emittance value that is larger than the real emittance.

The second assumption made in the optical determination of total
hemispherical emittance assigns to the sample the qualities of a gray-
body, an assumption required to obtain the directional total emittance
from the directional spectral emittance. The directional spectral
emittance was calculated from the NNISR measurement, as described in the
last paragraph. The directional total emittance is computed by inte-
grating the product of the directional spectral emittance and a black-
body distribution over all wavelengths. The limits of integration can
be reduced, however, to those wavelengths for which the blackbody
distribution is appreciably non-zero. For a sample at 150 C, these
limits are approximately 3 to 30 microns. At 50 C, the long wavelength
limit is closer to 40 microns. The directional spectral emittance,
calculated from NNISR, only covered the range of 2.5 to 15 microns, due
to the limited range of the spectrophotometer. To extrapolate the
directional spectral emittance out to the required wavelengths, we
assumed that the emittance would vary very little from the value corre-
sponding to 15 microns. This fixed fraction for emittance over the wave-
length band is the graybody assumption. The computed directional total
emittance would be larger or smaller than the real directional total
emittance, depending on whether the real directional spectral

emittance at wavelengths longer than 15 microns was larger or smaller

than the 15 micron value. Therefore, the effect of the graybody

assumption on the derived total hemispherical emittance can not be

determined unless more information on the NNISR or directional spectral

emittance is available for wavelengths longer than 15 microns.

The third assumption to be discussed is that emittance is a

function slowly varying with temperature. In the last paragraph, the

directional total emittance was computed by integrating the product of

the directional spectral emittance with a blackbody curve. If emittance

varies slowly with temperature, the calculated room temperature

directional spectral emittance can be used with blackbody distributions

for 50 C, 100 C, and 150 C, with little error. However, it is known

that emittance does change with temperature, and generally it increases.

This means that at higher temperatures, the calculated directional total

emittance is lower than the real directional total emittance.

The last assumption to be discussed is that there are no textural

or other surface effects that increase the total hemispherical emit-

tance. The directional total emittance calculated is actually a normal

total emittance, which can be converted to a hemispherical total emit-

tance by using the corresponding Fresnel ratio as described in Chapter

4. Surface roughness can increase hemispherical total emittance in two

ways. First, surface roughness can increase the actual radiating

surface area, allowing more radiation, which appears as an increase in

emittance. Second, surface roughness can create small cavities on a

surface that radiate like blackbodies with high emittance. The

emittance measured will be the sum of the material's emittance and the
high emittance of these cavities, which will be higher than the measured
emittance of a smooth sample.  Surface oxide layers also generally
increase the emittance of materials (Siegel and Howell, 1972).  Thus,
surface effects can result in a calculated hemispherical total emittance,
based on the normal emittance and the Fresnel relations, lower than
the real total hemispherical emittance.

We will now summarize these assumptions' effects on the derived
hemispherical total emittance before using this information to  analyze
the results listed in Chapter 7.  The specular assumption leads to an
emittance value too large.  The graybody assumption effect is indetermi-
nate unless more information is available about long wavelength
characteristics.  The assumption of emittance as a slowly varying
function of temperature leads to too low an emittance value at the
higher temperatures.  And finally, the effect of surface effects is to
derive an emittance value that is also too low.  All four of these
effects can be seen in the data presented.

The first of the data using the above analysis tools is another
verification of the accuracy of the CVE.  We know that vacuum deposition
of aluminum on an optically flat substrate produces a smooth, flat
surface.  Therefore, we do not expect to see surface effects.  The
measured total hemispherical emittance of aluminum varies little with
temperature, so another possible effect can be discarded.  Information
is available to analyze the effect of the graybody assumption.  The
Bennett group has published values of normal spectral reflectance of

aged aluminum out to 30 microns, measured under ultra-high vacuum with a high precision absolute reflectometer. Using this data the normal total emittance of aluminum at 150 C is 0.019 instead of 0.023 as measured by the Perkin-Elmer 137. Nevertheless, our normal total value was reasonably accurate. That our ratio of hemispherical total emittance to normal total emittance is lower than predicted by the Fresnel relations must therefore be the result of specularity. Aluminum is obviously a highly specular material. However, only a one percent non-specularity of aluminum would reduce the normal total emittance to 0.0102. Using this value in the ratio, $\epsilon/\epsilon_n$, results in value of 1.27, 1.27, and 1.37, which are close to the Fresnel predicted value of 1.30.

Even if our assumption of one percent non-specularity is wrong, the results show our hemispherical total emittance to be close to the actual value for aluminum. If we ignore specularity, and compute total hemispherical emittance from the Bennett data and the Fresnel ratio, we obtain an upper limit for the hemispherical total emittance of 0.0273, which is below all but the CVE data in Figure 6.1. Again, the conclusion is that the CVE is an accurate emissometer.

The nickel data shows the same effects. The ratios of hemispherical total emittance to normal total emittance are too low for the 50 C and 100 C values, compared to the Fresnel ratio. This is probably due to both the specular assumption and a decreasing emittance beyond 15 microns, just as in the case of aluminum. The higher than predicted ratio for nickel at 150 C is probably due to an actual increase in the emittance from room temperature to 150 C.

The ratios of hemispherical total emittance to normal total
emittance for all four molybdenum samples are higher than the Fresnel
predictions. The effect of assuming emittance as a slowly changing
function of temperature can be seen in all samples except for Black
Molybdenum #3. In the other samples, the ratios increased with in-
creasing temperature, just as predicted in the above discussion. The
other cause of the ratios being too high, surface effects, can be
justified simply by referring to Figure 2.3, a photograph of the surface
of Black Molybdenum, which shows the granularity of the surface. The
grain sizes range up to approximately micron and their size is a function
of the annealing time.

Annealing has two effects on these CVD molybdenum thin films.
Before annealing, the thin film is composed largely of molybdenum
dioxide. Annealing slowly drives the oxygen out of the film, which
drastically reduces its emittance. Annealing also increases the grain
size and creates voids, surface effects which result in higher total
hemispherical emittance (Carver, 1980). It can be seen that the re-
duction of oxygen occurs first. The three Black Molybdenum samples all
have approximately the same ratio of hemispherical total emittance to
normal total emittance, but Black Molybdenum samples #1, #2, and #3,
which were annealed for 3, 1, and 0 minutes, have 50 C hemispherical
total emittances of 0.103, 0.143, and 0.307. The emittances decrease
with longer annealing times. The Super Molybdenum samples have the
lowest hemispherical total emittances but the largest ratios of
hemispherical total emittance to normal total emittance. This can be

emplained by the annealing out of the thin film the last of the oxygen, which reduces the emittance, and the growth of the molybdenum grains, whose surface effect increases the ratio.

The value of the optical method of deriving hemispherical total emittance from NNISR can now be determined. Table 7.4 shows the relative error in emittance derived by the optical method. Table 7.1 contains values of total hemispherical emittance as derived by the optical method and determined by the calorimetric method. While the errors fluctuate from material to material, the optically derived emittances are, as a class, too low. The optical method could be improved somewhat, however, by the inclusion of additional data. The Optical Sciences Center has a scatterometer which can determine a material's bidirectional reflectance distribution function. This function could serve as an input to the material's specularity, thus eliminating one source of error. This device may also be able to provide a single spectral reflectance measurement at a long wavelength, i.e., 30 to 40 microns, which would help determine the effect of the graybody assumption. The surface smoothness can be determined by scanning electron microscopy, which could determine grain size and provide an input to surface effects. The only assumption left to generate error is that emittance is a slowly varying function of temperature. There simply is no means of quantifying this effect without performing measurements at the desired temperatures. This last assumption will probably be the limiting factor in the accuracy of the optical method of determining total hemispherical emittance.

CHAPTER 9

CONCLUSION

This thesis set out to meet the three goals stated in the first chapter. The importance of total hemispherical emittance to the total radiative loss of a material was stated for space and military applications, and shown for the solar photothermal conversion application. The relations between emittance and the other optical observable functions of n and k were derived. A means of determining total hemispherical emittance from a near normal incidence spectral reflectance measurement was shown and analyzed. A device to measure total hemispherical emittance, the Calorimetric Vacuum Emissometer, was constructed and shown to have a high degree of precision. Measurements were made of the total hemispherical emittance and total normal emittance of aluminum and nickel for calibration purposes, and of several different molybdenum thin films to evaluate their potential for the solar photothermal conversion process. Finally, a comparison of the optical and calorimetric means of determining total hemispherical emittance was made.

The comparison of the two methods of determining total hemispherical emittance was the subject of Chapter 8. The calorimetric method, which gave results with a minimum of assumptions, was used as

83

the standard against which the optical method was assessed. The optical method required the use of four approximations:

1. sample specularity was required to insure the measured near normal incidence spectral reflectance was all the reflected radiation from the surface.

2. the graybody assumption was used to extrapolate the NNISR to wavelengths beyond the range of the spectrophotometer,

3. the emittance was assumed to be a slowly varying function of temperature so that the optical method could derive emittance at temperature other than at which the NNISR measurement was made, and

4. surface effects were assumed to be neglible so that the Fresnel relations could be used to convert total normal emittance to total hemispherical emittance.

The effect of these assumptions was to introduce error in the derived total hemispherical emittance.

The assumptions listed above did not affect the assessment of the data in the same direction. The specular assumption consistently causes an emittance to be calculated too large. The graybody assumption effect can go in either direction unless additional information is available to characterize the observable quantities at wavelengths longer than the range covered by the spectrophotometer. The effect of assuming emittance to be a function slowly changing with temperature is generally assumed to underestimate the real emittance of the material. Finally, surface effects also result in emittance measurements below

actual values. This last effect dominated throughout the molybdenum thin films.

The results of the above analysis of the optical method of determining total hemispherical emittance suggests that the method be revised. The scatterometer of the Optical Sciences Center can be used to determine the specularity of the sample and to approximate the actual error resulting from the graybody assumption. Electron microscopy and other tests can quantify the surface effects. Only the effect of temperature on emittance cannot be determined without a measurement of the sample at the desired temperature. An improved optical emittance determination, using the above inputs, should result in a more accurate total hemispherical emittance determination from optical measurement.

APPENDIX A

OPERATION OF THE CVE

This appendix is devoted to a detailed description of the operation of the CVE. There are three main subdivisions of the opeation, sample insertion, vacuum system operation and data collection. After some hands-on experience, one person can perform the operation in a two-day cycle without great difficulty.

## Sample Insertion

Sample insertion requires opening the CVE, removing an old sample, inserting the new sample in the sample holder, and replacing the vacuum flange on the steel cylinder. The main difficulties are removing and replacing the flange, preferably done by two men, and not contaminating the sample in the process. The main tools for this step are a 9/16 inch open end wrench, a Phillips screwdriver, and a razor blade.

It will be assumed that the sample is prepared on a 3 x 3 inch square substrate. The corners of the sample need to be rounded to fit in the sample holder; quartz substrates can be trimmed by squeezing the vertex of the corner in a pair of pliers until the corner snaps off.

To open the CVE, first isolate the diffusion pump by closing the high vacuum valve. This is the valve that is between the diffusion

pump and the CVE chamber. The handle should be moved counter-clockwise until the overcenter lock is felt to click in place. The mechanical pump should be left backing the diffusion pump. The diffusion pump need not be shut off. The chamber is now isolated and can be brought to atmospheric pressure by opening the valve on the front of the vacuum flange.

Removing the vacuum flange requires a 9/16 open end wrench. Remove the two thermocouple vacuum gauge leads and the ion gauge tube. Then unscrew all but the top two bolds. This is where a second person is helpful. The flange must be supported while the last two bolts are loosened, and it is almost too heavy for one hand, so use caution. The vacuum flange, when removed, can be placed with the sample holder side up on the three armed support built out of 2 x 4's.

A sample in the holder is difficult to extract. Unscrew the four corner clamps, move the aluminum strips to the side and remove the four Teflon™ spacers. It must be done slowly to avoid damaging the thermopile! Use either the screwdriver or the razor blade to pry the edge of the sample out of the depression on the sample holder's face. On the thicker samples, the screwdriver works particularly well in the area where the thermopile leads exit. Once the sample edge is lifted, the thermopile usually needs to be separated from the sample's bottom surface. The danger is bending, and then breaking, the thermopile. The thermopile can be removed safely by sliding the razor blade between the two at a very shallow angle, and slowly lifting up on the thermopile leads. The bottom of the sample will be coated with vacuum grease.

Use care to avoid getting the grease on the thin film surface as ususally the sample needs to be tested for contamination after the CVE run.

The first step in mounting the new sample is to put on a plastic glove to avoid contamination. Hold the sample only by the edges and be careful. Coat the backside of the sample with vacuum grease; a bead of vacuum grease 1/2 inch long is the maximum amount necessary. Spread it evenly across all the back surface. Lay the sample on the thermopile on the sample holder. Clean the Teflon spacers with acetone and then place them on the four corners of the sample. Position the aluminum corner pieces on top of the Teflon and then gently screw them in place. Pressure may need to be applied to the Teflon spacers to keep them from being squeezed out of position with the final tightening of the screws. Tighten each screw only a little at a time to keep the application of pressure as even as possible.

Reassembling the CVE is simple. Check the large O-ring on the steel cylinder for cleanliness. If necessary, clean with acetone and reapply a thin coat of vacuum grease. With a helper if possible, bolt the vacuum flange back in place, taking care to mount the flange so that the sample holder is aligned with the opening in the sample cavity and with no wires touching the cavity. Tighten all the bolds, then connect the thermocouple vacuum gauge leads and the ion vacuum tube.

## Vacuum System Operation

Vacuum system operation is simple but the system needs many hours to reach the proper vacuum. As stated before, the paint used

inside the sample cavity outgasses terribly and this condition needs to be treated before data can be taken.

At this point, the sample is inside the chamber and the vacuum flange is bolted on. Insure that the relief valve on the flange is closed. Switch the mechanical pump from the backing position to the roughing position. In approximately five minutes, the vacuum in the chamber should be better than 50 millitorr. Switch the mechanical pump back to the diffusion pump and then open the high vacuum valve. The thermocouple gauges should be pegged at zero.

To outgas the paint, hot water is run through the sample cavity coils. In the lab, a sink is adjacent to the CVE, and is used for the source and disposal of hot water. The cavity is connected to the faucet by flexible rubber tubing, one end over the faucet and the other over the nearer cavity port. A second rubber hose connects to the cavity port on theother side and then runs over the CVE and into the sink. All connections are clamped for security, as the water is usually circulated overnight. The water pressure should not be high; adjust the pressure so that no, or very little, water leaks out from the base of the faucet. Once the water is turned on, the vacuum in the chamber will become poor. If the ion vacuum gauge is on, it may shut down. In one hour the vacuum improves significantly, and in 6 to 8 hours, the vacuum should be in the $10^{-6}$ Torr range.

At the same time the hot water is turned on, the power supply to the cartridge heaters should be adjusted to give enough power to heat the sample to approximately 150 C. A setting of approximately 200

milliamps and 80 volts will accomplish this. This will outgas the
sample and sample holder at the same time.

Disconnecting the water is simple. Turn off the water and
remove only the faucet connection. Place this end in the sink. Take
the other hose's free end and connet it to a compressed air source, such
as dry nitrogen. Purge the system until virtually all the water is out
of the sample coils. At 30-40 psi, this usually takes 3 to 5 minutes.
Then disconnect the hoses completely. At this point, the vacuum
should be better than $5 \times 10^{-6}$ Torr.

## Data Collection

Data collection is simple but tedious. Liquid nitrogen is run
through the sample cavity until the temperature of the sample stabilizes.
The temperature is noted along with the input power. From this data
the emittance can be measured. For three measurements, at 150 C, 100 C,
and 50 C, this process can take from seven to twelve hours. Although
the time required depends on the sample, the operator's experience is
the main shortcut.

First, the liquid nitrogen must be connected and circulated.
Approximately 30 to 40 liters of liquid nitrogen will be used, so check
the source accordingly. The dewar of liquid nitrogen is connected by
pipe fittings and copper tubing to the cavity port. Caution: The
male fitting on the cavity port is soft soldered. When tightening this
fitting, use two wrenches, one to hold the male fitting stationary and
the other to tighten the fitting. The copper tubing is wrapped with an

insulating material to cut thermal losses. From the other cavity port the tubing enters a small dewar. This was meant to collect the liquid nitrogen for recycling, but this proved too difficult. There is a valve on the fitting into the dewar that can be used to provide backpressure for the system. When the liquid nitrogen is first turned on, this valve should be fully open. When the fitting on the dewar starts to ice over, this valve should be closed until only a little gas escapes. The correct amount will leave the fitting just covered with ice. This slows the rate at which the nitrogen is consumed.

At this point, the sample will start towards an equilibrium temperature, since the power is constant and the environment has reduced all other heat sources. This is a lengthy process but experience can somewhat speed it. The power setting was already mentioned, 200 mA and 80 V. Generally, before the cooling with liquid nitrogen, this will result in a sample temperature above 170 C. For samples of low emittance, the equilibrium temperature will be approximately 150 C. To speed up the process, turn off the power supply and allow the sample to cool down to 160 C, then return the power to the previous setting. By the time the heat flow stabilizes again, the temperature will be close to the equilibrium temperature. Every 15 to 20 minutes check the zero setting of the microvoltmeter, the actual thermopile voltage, and the four sample temperatures. The thermopile reading will stabilize first. The criteria used for equilibrium have been either no change for 45 minutes or readings that fluctuate in temperature both up and down slightly. In the 150 C range, this usually takes approximately 2 hours.

After the 150 C data has been taken, turn off the power supply and allow the sample to cool to approximately 110 C. This will take around 30 minutes. Then turn on the power supply and set it to approximately 150 mA and 60 V. Again take readings every 14 to 20 minutes, and using the same criteria as before, the equilibrium temperature will be reached in about three hours.

For the 50 C data, again turn off the power supply until the sample temperature reaches approximately 60 C, then set the power supply at 125 mA and 40 V. This data point will take three or more hours. The vacuum usually starts to deteriorate at this point. Outgas the ion gauge for 10 to 15 minutes for an accurate reading.

When all three data points are taken, turn off the ion gauge, the liquid nitrogen, and the power supply. It is usually better to leave the sample in the chamber until the next day, to avoid moisture condensing on the cold cavity. Leave the vacuum pumps running.

This appendix has described the operation of the CVE. This information is summarized in a checklist in Figure A-1. Chapter 7 demonstrated that from this data, an accurate emittance can be calculated. The accuracy was shown both in an absolute sense, in that from Equation 5.1 no other terms are large enough to give any significant error, and in a relative sense, comparing CVE measurements with other known, published values.

Table A-1. Checklist for Operation of the CVE.

---

Sample Insertion

Obtain sample

Close high vacuum valve (directly above diffusion pump, handle moves counterclockwise)

Open air admittance valve (on front oe CVE)

Remove vacuum flange

Remove thermocouple connections and ion gauge

Use 9/16 wrench. CAUTION: flange is heavy

Remove old sample, razor blade or screwdriver. CAUTION: thermopile will stick to bottom of sample, do not damage!!

Mount new sample

Wear rubber gloves

Coat backside of sample with vacuum grease, a bead 1/2 inch long is sufficient, do not get grease on front

Clean Teflon™ spacers with acetone, then screw down corner supports and Teflon spacers on sample

Bolt vacuum flange back on CVE

Replace thermocouple leads and ion gauge

Close air admittance valve

Vacuum System Operation

Switch mechanical pump to roughing (position labeled on valve)

Wait approximately 5 minutes--vacuum > 50 millitorr

Switch mechanical pump to backing (labeled) and open high vacuum valve (clockwise)

Connect rubber tubing to faucet and liquid nitrogen ports on CVE

Table A-1.  Continued

---

**Vacuum System Operation (Continued)**

Turn on hot water, slightly more than a trickle, no spray from faucet

Turn on power supply--set to approximately 200 mA and 80 V

Wait several hours--overnight.  Vacuum $> 10^{-6}$ Torr

Disconnect water tubing from faucet, leave end in sink

Purge system with nitrogen gas until all water out of CVE

Remove all tubing

**Data Collection**

Connect liquid nitrogen--two large crescent wrenches

Run liquid nitrogen--adjust flow rate with valve on collection dewar

Wait approximately 1 hour, then take readings of temperature, thermopile every 15 minutes until readings are constant for 45 minutes.

Turn off power supply--allow sample to cool to next temperature

Turn on power supply--approximately 160 mA and 60 V

Wait 1 1/2 hours--then take readings as before

Turn off power supply to cool sample to third temperature

Turn on power supply--125 mA and 40 V

Take readings as before

Turn off power supply, ion guage, liquid nitrogen

Wait several hours or overnight to remove sample (reduces condensation on the cold copper tubing)

Table A-1.  <u>Continued</u>

| Temperature | Voltage | Milliamps |
|:-----------:|:-------:|:---------:|
| 150 C | 80 | 200 |
| 100 C | 60 | 160 |
| 50 C | 40 | 100 |

REFERENCES

Annual Book of ASTM Standards, "Standard Test Method for Total Hemi-
        spherical Emittance for 20 1400°C", American Soceity for
        Testing and Materials, Philadelphia, PA (1976).

Bennett, H. E., M. Silver and E. J. Ashley, "Infrared Reflectance of
        Aluminum Evaporated in Ultra High Vacuum, Journal of the Optical
        Sciety of America, Vol. 53, No. 9 (Sept 1963), pp. 1089-1095.

Carver, G. E. "Optical Properties of Chemical Vapor Deposited Moly-
        bdenum Thin Films". Ph.D. Dissertation, University of Arizona
        (1980).

Kittel, Charles, Thermal Physics, John Wiley, New York (1969).

Seraphin, B. E., Notes on a series of lectures presented at the 2nd
        International Symposium on Non-Conventional Energy conducted
        at the International Centre for Theoretical Physics, Trieste
        (Italy), (June 1981).

Siegel, R., and J. R. Howell, Thermal Radiation Heat Transfer, McGraw
        Hill Book Company, New York (1972).

Touloukian, Y. S., and D. P. DeWitt, Thermophysical Properties of
        Matter, Vol. 7. "Thermal Radiation Properties", Plenum, New
        York (1970).